State distribution in hydrogenated microcrystalline silicon

I. Balberg,[1] Y. Dover,[1] R. Naides,[1] J. P. Conde,[2] and V. Chu[3]

[1]*The Racah Institute of Physics, The Hebrew University, Jerusalem 91904, Israel*
[2]*Department of Material Engineering, Institutu Superior Technico, Av. Rovisco Pais, 1049-001 Lisboa, Portugal*
[3]*INESC Microsistemas e Nanotecnologias, Rua Alves Redol 9, 1000 Lisboa, Portugal*

We have been able to determine the density of states map in the band gap of a semiconductor by the measurement of the phototransport properties of its majority and minority carriers. In particular we found that the carrier recombination in *single-phase* hydrogenated microcrystalline silicon (μc-Si:H) is significantly different from the one in hydrogenated amorphous silicon (a-Si:H) and that it is controlled only by its two band tails. The comparison of the observed temperature dependence of the phototransport properties of this material with model simulations further suggests that, while the conduction-band tail has an exponential distribution of states, the valence-band-tail states have a Gaussian-like distribution. This, in turn, meets the challenge of the determination of the analytical shape of the density of states distribution from experimental data. Our experimental procedure implies then that this distribution is associated with the route through which the transport and phototransport take place and thus we conclude that both the recombination and transport in undoped single-phase μc-Si:H take place in the disordered layer that wraps the crystallites. We further conclude that, from the transport and phototransport points of view, the single-phase μc-Si:H is, in general, different from both polycrystalline silicon and a-Si:H. The polycrystalline-silicon-like behavior, when found, appears to be an asymptotic case in which the crystallites are large enough, while the a-Si:H behavior prevails only when there is a significant content of its phase within the system.

I. INTRODUCTION

Since the discovery of the higher efficiency and stability of solar cells based on hydrogenated microcrystalline silicon (μc-Si:H) this material has been studied intensively[1–3] from both the applications[1] (that utilize hydrogenated amorphous silicon technology) and basic physics[4–7] points of view. In spite of the corresponding wide interest in the transport and phototransport properties of this system[2] the understanding of these properties is still at a rudimentary level[4] and very little is known about the localized state distribution in it. The main problem in the basic understanding of this material is that its heterogeneous composition may contain, in principle, at least three well-defined phases. These are the silicon microcrystallites, the hydrogenated amorphous silicon (a-Si:H) and the voids. In addition there are the disordered silicon tissues, or the boundaries, between each two of the different phases.[2,8,9] Such are the boundaries between adjacent crystallites and disordered layers that encapsulate the columns of crystallites[8] that are formed upon the deposition of the μc-Si:H layers. In fact, μc-Si:H, as studied and described thus far, is actually a wide class of materials rather than a well-defined system.[8] This problem was often overlooked yielding questions such as "why is the transport in μc-Si:H so similar to that in a-Si:H?"[2] Hence, it is not clear if measured properties[9–14] that are usually similar to those found in a-Si:H are inherent in the μc-Si:H system or are they the contribution of the amorphous phase. For example, the transport properties were explained[13,15,16] by intercrystallite percolation models, conduction in the a-Si:H phase[17] and/or conduction via the above-mentioned layers.[12,18] Examples for the unclear situation are the works[10,11] in which the re-

sults can be identified as due to the presence of the a-Si:H phase, but the authors attributed them to be meaningful features of the heterogeneous μc-Si:H system. In the few cases where the contributions of the various phases were considered, general statements concerning the importance of the boundaries were usually given, but no specific models have been suggested.[5,7,12] Specific models were proposed only in very few studies.[8,13,14]

A fundamental issue that has not been resolved for the μc-Si:H systems is their density of states (DOS) map. While a few partial (only in the proximity of the conduction-band edge) DOS maps were proposed,[14,19] a full DOS map for any μc-Si:H systems has not been reported. In particular, since the system is ill defined, the states observed in the corresponding pseudogaps can be attributed to the various phases and boundaries. Of these, the contribution of the a-Si:H phase may be responsible for the observed dangling bonds, but these may also belong to the above-mentioned layers.[20,21]

Following the above considerations we have carried out a comprehensive study of the DOS in samples of the much simpler single-phase μc-Si:H system that we define here as a phase that consists only of silicon microcrystallites and their boundaries. This study is expected then to enable the distinction between the contribution of the network of the microcrystallites and the contribution of the a-Si:H phase in the heterogeneous systems that are commonly studied. In particular we expected that since our experimental method[22] involves transport and phototransport measurements, the derivation of a DOS map would also yield information on the transport routes in this system and shed light on the observations in the heterogeneous systems.

In this paper, we are able to show that the single-phase

μc-Si:H is very clearly distinguishable from a-Si:H in the behavior of its phototransport and to derive a full map of the states in μc-Si:H systems in general and in the single-phase material in particular. Our analysis shows that in our single-phase μc-Si:H the dominant recombination centers, as in chalcogenides,[23,24] are the band tails. In addition, we provide here an experimental confirmation of the Rose theory[25] for recombination in band-tail systems, and we meet the challenge[26] of an experimental determination of the analytical shape of the DOS of the band tails. The presently derived DOS map has then consequences on the understanding of the transport and phototransport properties of μc-Si:H, chalcogenide,[23,24] and porous[27] semiconductors.

The structure of this paper is as follows. In Sec. II we give the experimental details and in Sec. III we present the experimental results and discuss them. In Sec. IV we describe our comprehensive modeling study and in Sec. V we derive the most likely DOS map of the system at hand. Finally, in Sec. VI, we discuss the implication of the derived DOS map on the problem of the transport and phototransport routes and mechanisms in μc-Si:H.

II. EXPERIMENTAL DETAILS

It is well known[14,28,29] that under high hydrogen dilution various a-Si:H-like deposition methods yield μc-Si:H materials. In this work we have studied two sets of single-phase μc-Si:H samples prepared by the hot wire (HW) chemical vapor deposition technique under very high hydrogen dilution (90%). The second set was prepared under the same conditions but a year later in order to ensure the reproducibility of the experimental behaviors. Since the results were much the same we concentrate in this paper on those that we obtained on one of the samples. For comparison, we have also examined the phototransport of a-Si:H films prepared under exactly the same conditions (substrate temperature of 175 °C) but with no hydrogen dilution. The details of the latter study and its results have been presented previously.[22] The substrate we used for the study of the transport and phototransport properties was Corning 7059 glass. The preparation of our μc-Si:H samples and some of their room temperature structural, optical, and electrical properties have already been described.[28] In particular, the typical crystallite size in our samples is between 10 and 20 nm. For the present purpose, this and the fact that the Raman spectrum analysis has revealed *no a-Si:H phase in the μc-Si:H materials and no μc-Si:H phase in the a-Si:H materials* are of great significance.

Our transport studies were carried out using our standard two-probe (silver-evaporated) measurements[27] as a function of temperature. In our phototransport measurements[30] we have applied a He-Ne laser illumination that supplied a power of 7 mW, yielding a maximum generation rate, G, of 10^{21} cm^{-3} sec^{-1} carrier pairs. For the determination of the dependence of the phototransport properties on this rate we have varied G between that rate and 10^{19} cm^{-3} sec^{-1}. This relatively high generation rate is required in order to enable the linear conditions necessary for the application of the photocarrier grating technique.[30,31] The important point is, however, that we have used in the present study exactly the same conditions that we have applied previously in all our studies[22,30] of a-Si:H and in particular on the a-Si:H samples[22] that were prepared (apart from the hydrogen dilution) under the same conditions as the currently investigated single-phase μc-Si:H samples. This ensures that we reveal reliably the differences in the DOS maps of the two phases. The experimental technique and the derivation of the phototransport properties were as we have described in great detail previously.[22,30,31]

Briefly, we measured the photoconductivy $\sigma_{\rm ph}$, the light intensity (and thus the carrier generation rate G), the ambipolar diffusion length L, and the temperature T. We derived then the mobility-lifetime product of the majority carriers (here the electrons) from the relation $(\mu\tau)_e \equiv \mu_e(n-n_0)/G = \sigma_{\rm ph}/Gq$, where q is the electronic charge, μ_e is the electron mobility, n is the free-electron concentration, and n_0 is this concentration under equilibrium (in the dark). Similarly, we derived the mobility-lifetime product of the minority carriers (here the holes) from the relation $(\mu\tau)_h \equiv \mu_h(p-p_0)/G = qL^2/2kT$. Here p is the concentration of the free holes and p_0 is their concentration in the dark, and k is Boltzmann's constant. Assuming a power law dependence of $(\mu\tau)_e$ and $(\mu\tau)_h$ on G, we experimentally obtain the light intensity exponents γ_e and γ_h from the relations $\gamma_e - 1 = d[\log(\mu\tau)_e]/d[\log G]$ and $\gamma_h - 1 = d[\log(\mu\tau)_h]/d[\log G]$.

III. EXPERIMENTAL RESULTS

From the temperature dependence of the dark conductivity σ we found the significant parameters of the conductivity that is described by the relation $\sigma = \sigma_0 \exp(-E_a/kT)$. For temperatures above 200 K, the conductivity activation energy was found to be $E_a = 0.34$ eV and the conductivity prefactor was found to be $\sigma_0 = 5$ $(\Omega$ cm$)^{-1}$. Recalling the conventional consensus[5,12] that undoped μc-Si:H is n type, and using the common corresponding procedure[17,27,32] for the determination of the position of the dark Fermi level, E_F, with respect to the conduction-band edge, E_c [i.e., the enforcement of the prefactor of $\sigma_0 = 150$ $(\Omega$ cm$)^{-1}$], we got the value of $E_c - E_F = 0.46$ eV that we will apply below. This is in contrast with the $E_c - E_F = 0.65$ eV value that we obtained[22] for our "hot wire" a-Si:H material and the similar typical values obtained[30] for undoped a-Si:H.

Let us turn now to the results of the well-defined four phototransport properties[25,33,34] from which we derive in Sec. V the density of states distribution. Since all the evidence in the literature[5,35,36] is that undoped a-Si:H and undoped μc-Si:H are n-type photoconductors, we assumed that the measured $\mu\tau$ product of the majority carrier (i.e., the one that dominates the photoconductivity) is the mobility-lifetime product of the electrons. Correspondingly, we denote here the $\mu\tau$ product that is determined from the photoconductivity by $(\mu\tau)_e$. In Fig. 1(a) we show the typical temperature dependence of $(\mu\tau)_e$ of our single-phase μc-Si:H samples. We note first that the room temperature value obtained for this majority carrier $\mu\tau$ product is in excellent agreement with previous results[5,12,37] on μc-Si:H. More importantly, we see that, with the increase of the temperature there is a mono-
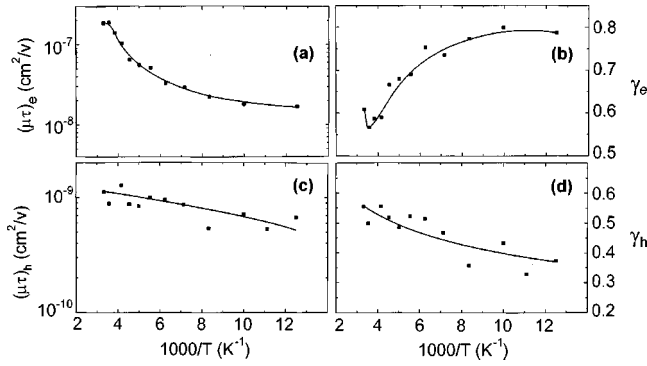
FIG. 1. Our experimentally determined temperature dependence of the four phototransport properties of a sample of single-phase microcrystalline silicon that was deposited by the chemical vapor deposition–hot wire technique. The curves are guides to the eye.

tonic increase of about an order of magnitude in $(\mu\tau)_e$. This is a very general behavior that is typical of recombination in both a single level[25,33] or band tails.[25,33,35] We further note that in contrast to this monotonic behavior, there is a non-monotonic behavior in systems where there is an appreciable concentration of dangling bonds. In those systems there is competition between the recombination in the dangling bonds and in a band tail. The latter process is accompanied then by the thermal quenching and sensitization phenomena[25,33] that are well known and quite well understood in a-Si:H.[22,30,33,36]

In Fig. 1(b) we see a monotonic decrease of the light intensity exponent γ_e with temperature. This result is consistent with the recombination in an exponential distribution of band-tail states.[25,26] The corresponding quantitative prediction of the simple theory of Rose[25] for such a distribution is that the value of γ_e is given by

$$\gamma_e = T_c/(T+T_c), \qquad (1)$$

where kT_c $(=E_{c0})$ is the width of the exponential conduction-band tail. The results shown in Fig. 1(b) are well fitted by a value of $kT_c=28$ meV. The value we found then is in excellent agreement with the well-known conduction-band-tail width in a-Si:H.[36] The increase of γ_e at higher temperatures is simply associated with the effect of thermally generated carriers, which will not be discussed here.

Both the results of $(\mu\tau)_e$ and γ_e show that there is no evidence for thermal quenching in the temperature dependence of $(\mu\tau)_e$ and for a corresponding sensitization that is known[22,25,36] to be manifested by a peak in the temperature dependence of γ_e with $\gamma_e>1$ values. Considering the fact that the present measurements were taken under exactly the same conditions that were applied to our HW a-Si:H samples,[22] the lack of these effects, in our present single phase μc-Si:H, suggests that there are no detectable dangling bonds here (see Sec. V). Rather, what we observe here appears to be a "pure" contribution of the conduction-band-tail states to the recombination. Support for this conclusion follows also from the partial DOS map that were deduced independently from photocurrent transients and modulated

photocurrent (MPC) measurements[14] and from the very large response times observed[38] in μc-Si:H.

Following these findings we note that the nature of the states through which the recombination actually takes place is not disclosed by the above-described results. In fact, we know[35] that such results reveal essentially only the nature of the states that enable the charge neutrality compensation, and not the ones in which the main recombination takes place. To find the latter states we must follow then the recombination in the states through which this process does take place. In other words, if we adopt the above picture of the conduction-band tail the above results cannot discern the states where the recombination actually takes place. The latter states can be revealed, however, by the study of the phototransport properties of the minority carriers, in our case, the holes.

The complementary measurement we are using is designed then for the determination of the phototransport properties of the holes, and these are associated with the state distribution in the rest of the pseudogap. In Fig. 1(c) we show the results of our measured $(\mu\tau)_h$ as a function of temperature. We see that there is a monotonic increase of the mobility-lifetime product of the minority carriers with temperature. The simultaneous monotonic increases of $(\mu\tau)_e$ and $(\mu\tau)_h$ is typical, as well as expected, in the presence of two band tails. Indeed, this is also the expected behavior of a-Si:H in the absence of dangling bonds.[35,36] In particular, as we will show here, the decisive information is derived mainly from the monotonic temperature dependence of the corresponding light intensity exponent of the minority carriers, γ_h. The temperature dependence of γ_h is presented in Fig. 1(d). Having the four dependencies of Fig. 1 we turned to deduce the DOS map in our single-phase μc-Si:H samples by a comprehensive study of model simulations.

IV. SOME DETAILS OF THE MODEL AND THE COMPUTER SIMULATIONS

In general, the model, the parameters, and the procedure that we used, for the derivation of the computed DOS map, were similar to those used by Tran for a-Si:H.[36] Our selection of the initial parameters followed, however, the information we had from our experimental study (see Sec. III) and/or values given in the literature. The motivation for the particular, but systematic, selection of some of the parameters is explained here and in the Appendix. We have carried out a very comprehensive model-simulation study for various DOS distributions in order to account for the experimental results given in Fig. 1. However, for the sake of brevity *we present here only some of our results*. In our simulation studies we went in fact beyond the scope that was considered by Tran by finding out the simplest model that can account for the data. We start with a brief outline of the model used in the simulations and then we introduce our computation procedure and the selection of the relevant parameters.

Consider a system of m types of centers of which the energy levels E_i are given within the band gap E_c-E_v, where E_c and E_v are the conduction- and valence-band edges.[33,36] These band edges have corresponding effective densities of states N_c and N_v. The concentration of each

type of centers is N_i and each type is characterized by its capture coefficients, C_{ni} for the electrons and C_{pi} for the holes. Under a given T and G there are steady state concentrations of $n - n_0$ photoexcited electrons and $p - p_0$ photoexcited holes where n_0 $(= N_c \exp\{-[(E_c - E_F)/kT]\})$ and p_0 $(= N_v \exp\{-[(E_F - E_v)/kT]\})$ are their corresponding concentrations in the dark. Correspondingly, the concentration of electron occupied centers of type i under illumination is n_{ti} and in the dark it is n_{ti0}. The generation-recombination processes (at E_c, E_v, and each E_i) can be presented by $m + 1$ independent equations. In the steady state we have at E_c the generation of G electrons as well as the thermal generation from all types of centers, Σg_{ci}. These are balanced by the recombination rates at all these centers Σr_{ci}:

$$G + \Sigma g_{ci} - \Sigma r_{ci} = 0. \tag{2}$$

Similarity at each energy level the balance of thermal generation and the recombination yields that for each i,

$$r_{ci} - r_{vi} + g_{vi} - g_{ci} = 0, \tag{3}$$

where r_{vi} is the rate of the recombination of the holes and g_{vi} is their thermal generation. The other equation that has to be fulfilled is the charge neutrality condition that can be written as

$$n - n_0 - p + p_0 + \Sigma n_{ti} - \Sigma n_{ti0} = 0, \tag{4}$$

where $n_{ti0} = N_i f(E_i - E_F)$ and $f(E) \equiv 1/[1 + \exp(E/kT)]$. We have then $m + 2$ independent equations with the $m + 2$ unknowns, n, p, and n_{ti}. In the above equations $g_{ci} = n_{ti} e_{ni}$ (where $e_{ni} = C_{ni} N_c \exp[-(E_c - E_i)/kT]$, $r_{ci} = C_{ni} n (N_i - n_{ti})$, $g_{vi} = (N_i - n_{ti}) e_{pi}$ (where $e_{pi} = C_{pi} N_v \exp[-(E_i - E_v)/kT]$) and $r_{vi} = C_{pi} p n_{ti}$. To find the unknowns one has to solve Eqs. (2)–(4). We express the mobility-lifetime products from the solved n and p as for the experimental case by $(\mu\tau)_e = \mu_e (n - n_0)/G$, and $(\mu\tau)_h = \mu_h (p - p_0)/G$ and the light intensity exponents by $\gamma_e - 1 = d[\log(\mu\tau)_e]/d[\log G]$ and $\gamma_h - 1 = d[\log(\mu\tau)_h]/d[\log G]$.

The above set of equations is well known and was used in numerous simulations.[22,33,36] For the present work we are concerned in particular with two special sets of centers that fit into the above framework with some simple particular modifications. We start with the correlated case of the dangling bonds.[36] These bonds constitute three possible states: A positively charged donorlike state D^+ with an energy E_{db}, a neutral state that also lies at E_{db}, and a negatively charged acceptorlike state D^- that lies at $E_{db} + U$, where U is the correlation energy. The occupation statistics of the states is determined by the corresponding "sum rule" of the occupation probabilities $F^+ + F^0 + F^- = 1$, where[33,36]

$$F^+ = \{1 + [(e_{p+} + nC_{n+})/(e_{n0} + pC_{p0})]$$
$$\times [1 + (e_{p0} + nC_{n0})/(e_{n-} + pC_{p-})]\}^{-1},$$

$$F^0 = \{1 + (e_{n0} + pC_{p0})/(e_{p+} + nC_{n+})$$
$$+ (e_{p0} + nC_{n0})/(e_{n-} + pC_{p-})\}^{-1}.$$

Here the subscript n indicates the capture and emission of electrons and the subscript p indicates the capture and emission of holes. The second subscript indicates the initial charge state of the dangling bond. The emission rates, as above, are determined by the capture and emission under equilibrium and are given by $e_{n0} = n_0 f_{0+} C_{n+}/f_{00}$, $e_{n-} = n_0 f_{00} C_{n0}/f_{0-}$, $e_{p0} = p_0 f_{0-} C_{p-}/f_{00}$, and $e_{p+} = p_0 f_{00} C_{p0}/f_{0+}$ where the corresponding occupancy functions f_{0+}, f_{00}, and f_{0-} are given by $f_{0+} = \{1 + 2\exp[(E_F - E)/kT] + \exp[(2E_F - 2E - U)/kT]\}^{-1}$, $f_{00} = \{2\exp[(E_F - E)/kT]\} f_{0+}$, and the sum rule $f_{0+} + f_{00} + f_{0-} = 1$. Here, the first zero in the subscript indicates that the quantity is under equilibrium condition, while the second subscript represents the charge state of the dangling bond.

The net recombination process at D^+ is determined by the capture rate of electrons $U_1 = nC_{n+}$ and the emission rate of holes e_{p+}, while the recombination rate at D^- is determined by the capture rate of holes pC_{p-} and the emission rate of electrons $U_4 = e_{n-}$. At D^0 all four processes [see Eq. (3)] take place; in particular, we recall the capture $U_2 = nC_{n0}$ and the emission $U_3 = e_{n0}$ of the electrons. Considering the electrons, the contribution of the dangling bonds to the general generation-recombination equation [Eq. (2)] is given by $G = U_1 + U_2 - U_3 - U_4$. Correspondingly, the change in the negative charge in the dangling bonds due to the illumination [that has to be added into the charge neutrality condition, as given by Eq. (4)] is $N_{db}[F^0 + 2F^- - f_0 - 2f_0^-]$, where N_{db} is the total concentration of the dangling bonds.

In our simulations, in addition to those presented in previous reports,[22,30] we also evaluated the recombination at each of the dangling bond states as well as the concentration of occupied centers of these states. Of course, the concentrations of electron occupied dangling bonds D^0 and D^- are given by $N_{db} F^0$ and $N_{db} F^-$, and the corresponding recombination rates are $N_{db} n F^+ C_{n+}$, $N_{db} F^0 (nC_{n0} - e_{n0})$, and $N_{db} F^- e_{n-}$. We note then that we can consider each dangling bond state separately in Eqs. (2) and (3), but since their occupation is correlated we must include their effect simultaneously. This is done by the above inclusion of ΣU_i and the charge neutrality condition in the global (conduction-band or valence-band edge) recombination equation.

Let us turn now to the generalization of the above model to a set of centers that constitute a continuous distribution of states $N_t(E)$. In this case, considering the detailed balance at each energy E, we have from Eq. (3) that the occupation probability f_t is given by $f_t(E) = n_t(E)/N_t(E) = (C_n n + C_p p)/[C_n(n + n_s) + C_p(p + p_s)]$, where $n_t(E)$ is the concentration of the electron occupied states at E and $N_t(E)$ is the total concentration of such states, $n_s = N_c \exp[-(E_c - E)/kT]$, and $p_s = N_v \exp[-(E - E_v)/kT]$. The total concentration of electron occupied states in the above distribution is given by

$$n_t = \int N_t(E) f_t(E) dE, \tag{5}$$

where the integration is over the entire band gap $E_c - E_v$. Under equilibrium $f_t(E)$ is simply the Fermi-Dirac function

$f_{t0}(E)$ and the total concentration of electron occupied states is

$$n_{t0} = \int N_t(E) f_{t0}(E) dE. \tag{6}$$

The effective contribution of this type of states to the charge neutrality equation [Eq. (4)] is then $n_t - n_{t0}$. The corresponding net recombination rate through each level is as in the single-level case and is derived from Eq. (3) by noting that the concentration of holes at E is $N_t(E) - n_t(E)$. For the case of the continuous distribution of states we get

$$r_c - g_c = \int N_t(E)[C_n C_p(np - n_0 p_0)]/[C_n(n + n_s) + C_p(p + p_s)] dE. \tag{7}$$

The main state distributions that we have considered in the present work were those of the exponential conduction-band tail and the Gaussian valence-band tail. The former is defined by

$$N(E) = N_{ct0} \exp[-(E_c - E)/E_{c0}], \tag{8}$$

and the latter is defined by

$$N(E) = N_{vt0} \exp[-(E - E_v)^2/2G_{v0}^2]. \tag{9}$$

Here N_{ct0} and N_{vt0} are the DOS values at E_c and E_v, respectively, while E_{c0} and G_{v0} are the corresponding widths of the above distributions.

Turning to the parameters used in the numerical simulations we point out that in our initial choice of parameters we have used the following procedure. When we had an experimentally determined parameter we carried out the initial computation with this parameter. Then, after we derived the other parameters, from the trials to fit the results of Fig. 1, we rechecked the effect of our initial choice on these parameters and we reconsidered them. For parameters for which we could only guess their values (such as the capture coefficients of the states[25,33,36]) we run our simulations with various plausible values. Since we have here the experimental value of $E_c - E_F$ we did not try to determine E_F from the DOS model[36] and assumed that there are very shallow donors that in combination with the suggested DOS map yield the experimentally observed value of $E_F - E_v$. The other parameter associated with the energy scale of the system is of course the energy gap. Considering initially (see the Appendix) a disordered semiconductor with a pseudo-band-gap, E_g, of 1.8 eV, we found that the results are not sensitive to the value of E_g. For the values of the mobilities, we have taken initially constants independent of temperature (for which there is also some evidence[13,15] in μc-Si:H) in order to concentrate on the recombination mechanism that yields (in particular via the mobility-independent quantities γ_e and γ_h) the DOS map. For the electrons, a completely independent study[39] on our samples suggested that the drift mobility in our system is of the order of 1 cm^2/V sec. This gave us our anchor for the mobility value used in the simulations. As we will see in Sec. V the important parameter involved, how-

ever, is the ratio of the electron to hole mobilities. In μc-Si:H the corresponding ratios reported[5,40,41] range between 1 and 200. Of course the derivation of the free carrier mobility from the various experiments in disordered semiconductors is not a resolved issue[42] and thus we have used this ratio as a fitting parameter.

As we pointed out above the well-known attempt in simulations such as ours[31] is to solve the concentrations of electrons, n, and holes, p, under the application of illumination, i.e., under a given carrier generation rate. In our measurements this was in the range between $G = 10^{19}$ and 10^{21} cm^{-3} sec^{-1}, and thus (while we have checked the effect of G on the results) we have chosen for this paper to present only the results for $G = 5 \times 10^{19}$ cm^{-3} sec^{-1}, noting that, as will be mentioned in Sec. V, the qualitative behavior of the simulation results was not too sensitive to the particular choice of G in the above experimental range.

Assuming then a given DOS distribution with its corresponding parameters we solved the above kinetic steady-state and charge neutrality equations by applying the Newton-Raphson method for finding the roots of n and p.[43] In the numerical calculation of the integrals (5)–(7) we have applied Simpson's method for numerical integration.[43] Once n and p were found we expressed the results by $(\mu\tau)_e \equiv \mu_e(n - n_0)/G$ and $(\mu\tau)_h \equiv \mu_h(p - p_0)/G$. The corresponding light intensity exponents were simply determined for $\gamma_e - 1$ and $\gamma_h - 1$ as explained above.

Last but not least, it is important to emphasize that we observed that our requirement for a simultaneous fit of the temperature dependence of *all* four phototransport properties with the experimental results is stringent enough to reduce the model-parameter space very significantly.[30] This was to the degree that, of the many possible scenarios, only the above-mentioned two [Eqs. (8) and (9)] can be considered to be the simplest plausible scenarios in our samples.

V. RESULTS OF THE MODEL SIMULATIONS

A. Preface

We start the review of our simulation study by noting that the present experimental results, in particular the $\gamma_h < 1/2$ value, cannot be a result of a recombination in a single-level center or a collection of discrete recombination levels of the same type[33,36] (say, donorlike centers). The need to assume then a system more complex than the single-level centers on the one hand, the expectation of a continuous distribution of states in such a disordered system as μc-Si:H, on the other hand, and the perfect agreement of the $\gamma_e(T)$ behavior with the simple theory of Rose[25] leave little doubt that at least one continuous distribution of states, i.e., a band-tail state distribution, must exist in our material. According to that theory, as given by Eq. (1), the behavior we observe for $\gamma_e(T)$ in Fig. 1(b) appears to represent an exponential conduction band tail[25,35] with a width of $E_{c0} = 0.03$ eV. Since the temperature dependence of γ_e is, in principle, determined[35] by the combination of both the energy dependence of the DOS in the conduction-band tail and in the valence-band tail, we have checked the above conclusion thoroughly by also assuming discrete levels, exponential band tails, Gaussian band

tails, steplike band tails, and exponential "square-root-like" band tails (see definitions in the Appendix) for the conduction band tail. In all these cases the results, in particular the $\gamma_e(T)$ and $\gamma_h(T)$ dependencies, were very different from the monotonic behaviors shown in Fig. 1. Consequently, and in accord with the existing analytical theories,[25,35] we view the observed $\gamma_e(T)$ dependence as well accounted for by an exponential conduction-band tail, and thus as a salient feature of the DOS map of the samples under study. We further found then that it was *only* the case of donorlike states in the conduction-band tail that enabled (for all the state distributions that we have tried for the rest of the pseudogap) the derivation of computed results that resemble the experimentally observed $\gamma_h(T)$ dependence. Hence, the other salient feature that we concluded from the experimental data was that of donorlike states in the conduction-band tail, and thus *we show below only* the results for which such a character has been assumed for the conduction-band tail states. In what follows we present the results of the three model maps that enabled us to conclude the most likely DOS map scenario for the single-phase μc-Si:H samples that we studied here. Also, as pointed out in Sec. III, it appears from the absence of thermal quenching and sensitization effects in the experimental results that the concentration of dangling bonds is negligible in comparison with that of other states. Hence, we assume initially that there are no dangling bonds in the system, showing later that this initial assumption is well justified. The sensitivity of the results to the choice of a parameter will be presented, however, by showing results for three parameter values.

B. Two exponential band tails

We start the presentation of the results of our simulations by showing a typical case that yields a clear disagreement with the experimental behavior shown in Fig. 1. The case that we have chosen to show follows the results that were obtained with the most obvious complementary type of recombination centers,[36] i.e. acceptor-like centers that belong to an exponential valence band-tail.

In Fig. 2 we show, as an example, the computed four phototransport properties as a function of temperature for a model that contains an exponential conduction-band tail, with a width of 0.03 eV and donorlike states, in addition to an exponential valence-band tail of acceptor-like states. We illustrate the DOS distribution, $g(E)$, of this model for three valence-band-tail widths in the right column of the figure. These DOS maps are derived by considering all the states that participate in the recombination at our $G=5 \times 10^{19}$ cm^{-3} sec^{-1} generation rate and at 15 K. The latter conditions enable the map to include practically all the states in the pseudogap. As is clearly seen for the reasonable range of exponential valence-band-tail widths (i.e., in the range of 10^{-3} to 10^{-1} eV), E_{v0}, the results are in conspicuous disagreement with the experimental results of Fig. 1. In particular, we found that changes in the capture coefficients (within the reasonable limits of 10^{-6} to 10^{-15} cm^3 sec^{-1}) or in the generation rate (within our experimental range) have been found to affect some features of the results shown in Fig. 2

but not in a manner that can enhance significantly the resemblance between the computed behaviors and the experimental dependencies shown in Fig. 1. Also, reversing the nature of the types of states in the two band tails yielded results that were even further away from the experimental behavior. Correspondingly, we conclude that the state distribution in the vicinity of the valence band is not exponential band-tail-like.

C. Conduction-band tail and discrete-level centers

Following our attempt to map the distribution of the other (beyond the conduction-band tail) states in the pseudogap, we turned to the simplest possibility, the one that can be an effective representation of a continuous distribution, i.e., that of centers with a single discrete level in the vicinity of E_v. Looking for an initial value for the concentration of such centers, we noted that in our recent work[22] on the corresponding a-Si:H samples (see Sec. II) we found a concentration of about 10^{18} cm^{-3} discrete-level acceptor states, N_{ta}. For these acceptors the capture coefficient for the electrons C_{na} was taken to be 10^{-8} cm^3 sec^{-1} and the capture coefficient for holes C_{pa} was taken to be 10^{-6} cm^3 sec^{-1}. Following that finding and the importance of starting from the simplest plausible model, we turned to check whether such a concentration of single-level acceptor states could be responsible for the behavior observed in Fig. 1. Later, as will be described below, we reexamined this initial value of N_{ta}.

We have carried out then the simulations for a wide range of the energy level of the states, E_{ta}. Our optimal selection of E_{ta} was based on results such as those shown in Fig. 3 for three plausible positions of E_{ta} (which are presented in the right column of the figure). It is seen from these results that our best choice is the case shown in the second row of the figure, i.e., that of $E_{ta}=0.125$ eV. We found that this fit with the qualitative behavior shown in Fig. 1 becomes noticeably worse as we try E_{ta} values outside the 0.125 ± 0.030 eV interval (for a better quantitative fit, however, see below). Having the latter value as an initial guess for E_{ta}, we returned to reexamine the value that we have chosen initially for N_{ta}. The determination of the corresponding optimal value was done then with the help of results such as those shown in Fig. 4. As we see, for $N_{ta}>10^{18}$ cm^{-3}, there is a very good fit with the behavior shown in Fig. 1.

Following the above results the question that arises is whether we can still get a better quantitative agreement with the experimental data by considering possible temperature dependencies of some of the phototransport parameters. To illustrate the possible effects of such temperature dependencies of the mobility[44] and/or the capture coefficient[45] on the behavior shown in the second row of Fig. 3 we present the corresponding results in Fig. 5. For the mobilities [Fig. 5(a)] we have used the values $\mu_e=(300/T)^{1.5}$ and $\mu_h=10^{-3}(300/T)^{1.5}$ cm^2/V sec, while for the capture coefficients of the discrete-level states [Fig. 5(b)] we have used the values $C_{na}=10^{-8}(T/300)^2$ cm^3 sec^{-1} and $C_{pa}=10^{-6}(T/300)^2$ cm^3 sec^{-1}. This is instead of the constant values (10^{-8} and 10^{-6} cm^3 sec^{-1}) that we used for the derivation of Figs. 3 and 4. These latter phenomenological representations improve the temperature dependence of the $\mu\tau$
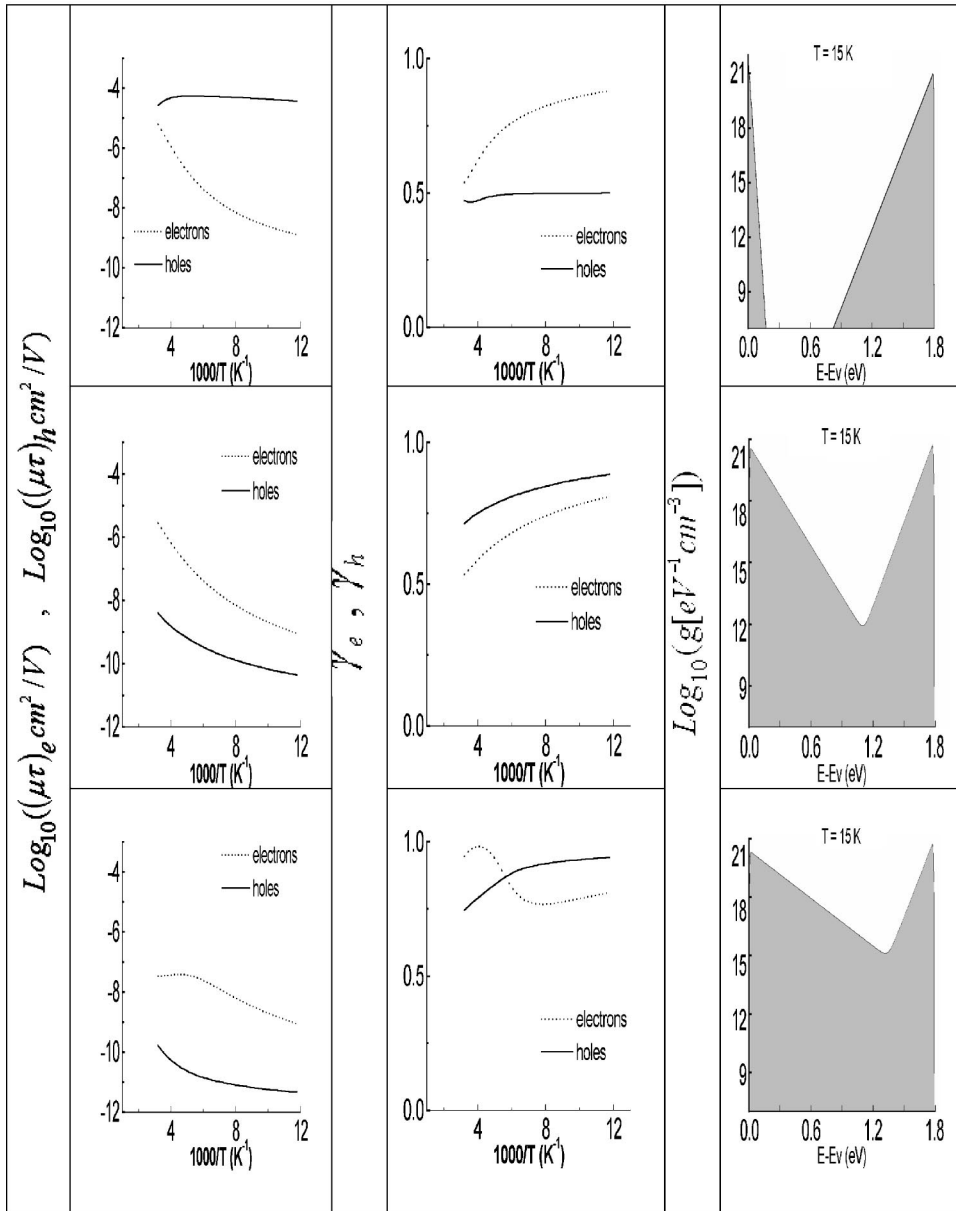
FIG. 2. The simulated temperature dependence of the four phototransport properties for the same conduction band tail but for three widths (0.005, 0.05, and 0.1 eV) of the exponential band tail of the valence band. Note that the third column represents the corresponding DOS in the pseudogap.

products so that they become quantitatively very close to the results shown in Fig. 1. It seems to us, however, that the most likely explanation for the quantitative discrepancy, in the strength of the temperature dependence of the $\mu\tau$ products, between the experimental results and the results given in the second row of Fig. 3 is due to the effect of thermal fluctuations on the effective DOS for recombination.[46] Such an effect has been considered already in works on a-Si:H.[46,47] Assuming a band tail with a width that increases faster at higher temperatures has already been shown[47] to lead to a weaker temperature dependence of the $\mu\tau$ products in comparison with the case for which this effect has not been considered. In fact, support for this explanation follows the observation that using this assumption led to a much better agreement with experimental results in the case of a-Si:H.[47]

Another important issue is the values of the mobilities of the two carriers that we have chosen in order to fit the ex-

perimentally derived magnitudes of the $\mu\tau$ products. Carrying out intensive simulations in order to check whether we can get a quantitative fit with mobilities such as those in a-Si:H, we changed the capture coefficients of either or both carriers. This study led us to the conclusion that such changes cannot yield the desired agreement with the experimental results and we were forced to assume large mobility ratios of $\mu_e/\mu_h = 10^3$. The important consequence of this interesting result is that in our system, under the assumed generation rates and temperature range, we have that $p - p_0 > n - n_0$, and that it is only the large μ_e/μ_h ratio that makes electrons the majority photocarriers. This rather unexpected result will be discussed in more detail in Sec. VI.

As for the parameters for which we had initial values, i.e., $E_F - E_v$ and G, we found that for our "best" fitted parameters of $E_{ta} = 0.125$ eV and $N_{ta} = 10^{18}$ cm^{-3} the results were much the same as in the range of $1.0 \leqslant E_F - E_v \leqslant 1.3$ eV. For higher $E_F - E_v$ values ($E_F - E_v \geqslant 1.5$ eV) we got, however,
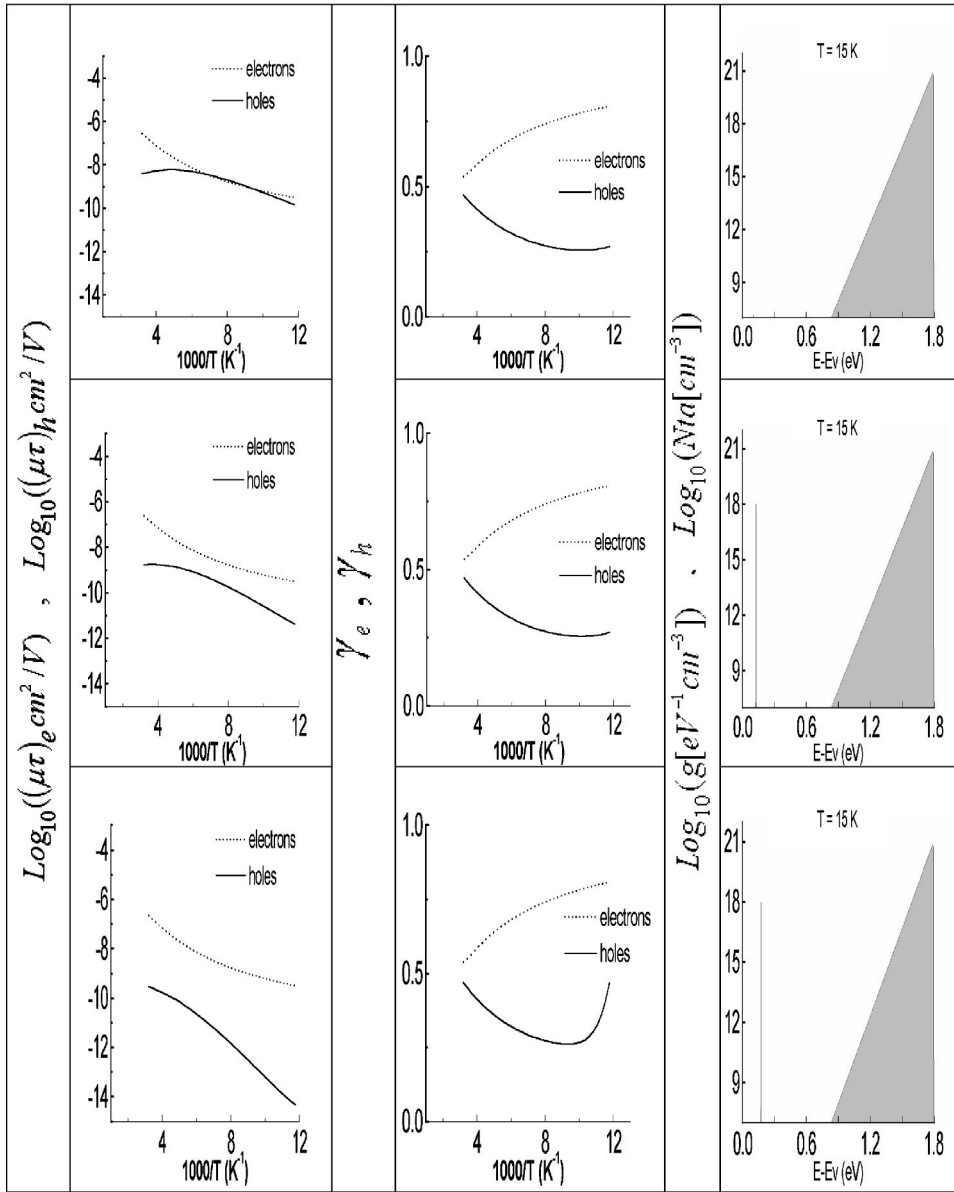
FIG. 3. The simulated temperature dependence of the four phototransport properties for three possible positions of the energy level, of 10^{18} cm^{-3} acceptorlike centers, that lies close to the valence band. The second row corresponds to the intermediate value of $E_{ta} = 0.125$ eV. In the third column we show the DOS for the continuous state distribution, $g(E)$, and the concentration of the single-level acceptorlike centers N_{ta}.

considerable deviations from the behaviors shown in Fig. 1 and in the second row of Fig. 3. For the carrier generation rate we found that the results are not too sensitive to the values of G in the range $10^{17} \leq G \leq 10^{21}$ cm^{-3} sec^{-1}.

In order to find out how well can we establish that the DOS map found here is different from that of a-Si:H, we have added dangling bonds to the model of our ''best'' case (second row of Fig. 3, $E_{ta} = E_v + 0.125$ eV) by applying the dangling bond model and the dangling bond parameters of Tran[36] (see Sec. IV and the Appendix). Some results of the corresponding study are shown in Fig. 6 for three concentrations of dangling bonds N_{db} (10^{14}, 10^{15}, and 10^{16} cm^{-3}). In this figure we show, in the first two columns, the computed phototransport parameters as in Figs. 2–4 and in the right column we have added to our ''best'' case (the DOS of the second row of Fig. 3) the concentration of dangling bonds. One notes that for the position of E_F and the very low temperature chosen, all the dangling bonds are negatively charged and thus N_{db} is represented by the discrete line at

$E - E_v = 1.25$ eV. As seen from the comparison of these results and the results in Fig. 1, only for N_{db} values larger than 10^{14} cm^{-3} will the effect of the dangling bonds be noticeable in the experimental data. This suggests that for all practical purposes *there are no dangling bonds* in our samples.

It is important to point out again that for all the simulations, the results of which are shown in Figs. 3–6, we found that a change of the character of the valence-band-tail states from acceptorlike to neutral-like or even to donorlike did not change the results in any significant way. But again, changing the character of the conduction-band-tail states to neutral-like or acceptorlike yielded very significant deviations from the experimental behaviors of $(\mu\tau)_e$, $(\mu\tau)_h$, and $\gamma_h(T)$.

In order to get a better understanding of the recombination process, we show in Fig. 7 the temperature dependence of the total concentrations of free carriers as well as the concentrations of carriers in the defect states (electron-empty acceptorlike and electron-occupied donorlike) that are neu-
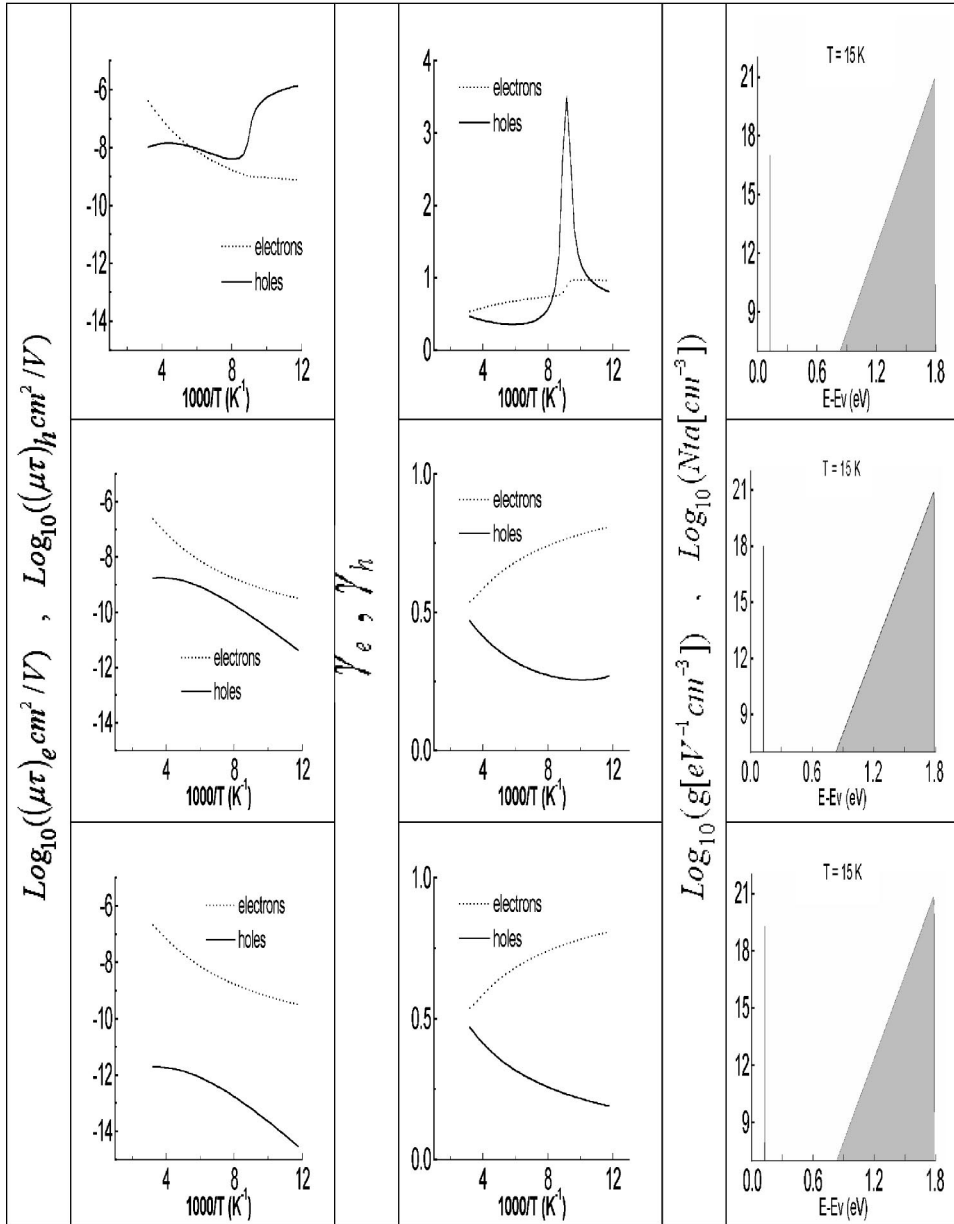
FIG. 4. The simulated temperature dependence of the four phototransport properties for three concentrations of the acceptor-like states (10^{17}, 10^{18}, and 10^{19} cm^{-3}), the level of which lies at $E_a = 0.125$ eV.

tral [Fig. 7(a)], as well as the recombination rates via the defect states [Fig. 7(b)]. These concentrations of holes in the acceptor level, P_{ta} [$= N_i - n_{ti}$, where $i = a$ in Eq. (4)] and electrons in the donor levels, N_{ct} [$= n_t$ in Eq. (5) with the substitution of $N(E)$ of Eq. (8) as $N_t(E)$], were obtained for our standard generation rate of $G = 5 \times 10^{19}$ cm^{-3} sec^{-1}. We note from the equality of N_{ct} and P_{ta} that N_{ct} is simply the concentration of electrons that have been transferred to the conduction-band tail from the acceptor states, under the applied G. As to be expected, from the relatively small concentrations of free carriers, this is the result of our charge neutrality condition. In Fig. 7(b) we see that the dominant recombination is via the acceptorlike states, G_{ta} [$= r_i - g_i$ for $i = a$; see Eq. (2)] rather than via the conduction-band-tail states, G_{ct} [$= r_c - g_c$, for $C_n = C_{nc}$ and $C_p = C_{pc}$; see Eq. (7)]. This is a *clear demonstration* of the Rose model[25] and its extension[35] in which the charge neutrality requirement and the position of the Fermi level force the above $T_c / (T_c$

$+ T)$ behavior [Eq. (1)] to be determined by the width of the conduction-band tail, in spite of the fact that the dominant recombination takes place elsewhere.

To further demonstrate the effect of the temperature on the distribution of the recombination-available centers we show in Fig. 8 the DOS map of the active recombination centers (that are responsible for the results shown in Figs. 3, 4, 6, and 7) for three temperatures. The gray area represents the collection of states that participate in the recombination for our "standard" case of $N_{ta} = 10^{18}$ cm^{-3} and $E_{ta} - E_F = 0.125$ eV. The results show the systematic decrease of the concentration of both types of such effective centers when the temperature is increased. These results stress in particular the increase in the occupation of the active band-tail states with decreasing temperature (and/or the increase of G) and show how the energy range of these states is broadened with decreasing temperature. In fact, the peak in the conduction-band-tail states is a demonstration of the Rose[25] concept of
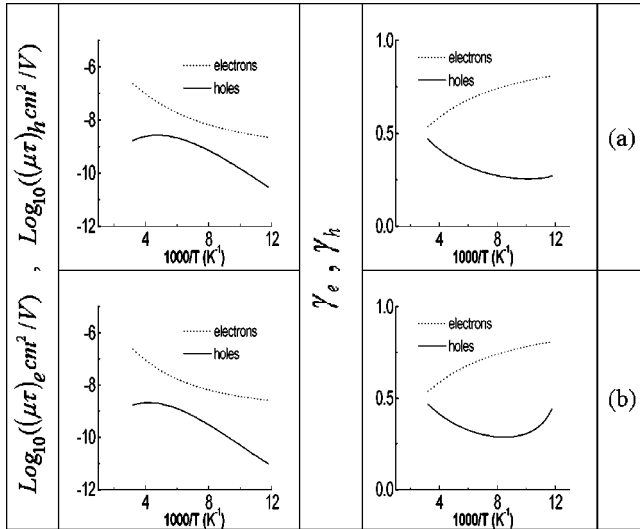
FIG. 5. Results such as those in Figs. 3 and 4 for E_a $=0.125$ eV and $N_{ta}=10^{18}$ cm^{-3} but with temperature-dependent mobilities (a) or temperature-dependent capture coefficients (b).

the demarcation level for a continuous distribution of states. The demarcation level separates states the occupation of which is controlled by recombination (the deeper-lying states) and states the occupation of which is controlled by "thermal excitation" or "thermal communication" with a band edge (the shallow states). We demonstrate the manifestation of the continuous character of this concept in contrast with the abrupt change that was considered in the simple analytic theory of Rose. The position of the observed peak can be defined then as the demarcation level in the case of a continuous distribution of states.

D. Gaussian valence-band tail

Let us turn now to the DOS maps that are more naturally expected for a disordered semiconductor. We know that, depending on the nature of the disorder that prevails in the semiconductor, various types of band tails other than exponential tails are plausible.[26,48,49] Following our systematic study of two exponential tails (see Fig. 2), two square-root-like tails, two steplike tails or combinations of an exponential with a square-root band tail or with a steplike band tail (see Ref. 46 as well as the Appendix for definitions) we concluded that (with any reasonable set of parameters) one cannot reproduce the behavior shown in Fig. 1. On the other hand, we were able to find a very strong resemblance between our simulation results for two band tails and this behavior when we assumed a model that included our above-given standard conduction-band tail and a Gaussian valence-band tail. Correspondingly we show here only the results obtained with the latter DOS map.

Before we describe our results, let us recall that for the conduction-band tail we have used as a parameter the well-known[44] effective density of states at E_c. Similarly, we use here the corresponding DOS value at E_v (with a value that is well accepted also for disordered silicon systems[36]), i.e., $N_{vt0}=10^{21}$ cm^{-3} eV^{-1}. The parameter we need here (of

which we have no prior knowledge) is the width of the Gaussian valence-band tail, G_{v0}. To find this parameter we searched the reasonable range of $10^{-1}\geq G_{v0}\geq 10^{-3}$ eV.

For a better quantitative agreement with the experimental $\mu\tau$ values we have chosen here a μ_e/μ_h ratio of 10^4 rather than 10 or 100, which is the typical[36] ratio chosen for a-Si:H, or the 10^3 ratio, which we have chosen above for the discrete-level case. This, as pointed out already, is not a trivial result since its implication is that it is the mobility that makes the single-phase μc-Si:H an n-type photoconductor. While initially unexpected we may note that μ_e/μ_h ratios as large as 200 have been reported[41] for μc-Si:H. In our case we may attribute the particular high ratio to the narrow valance-band tail that we find here.

The result of our attempt to estimate then the value of G_{v0} is presented in Fig. 9 where we show the temperature dependence of the phototransport properties for three Gaussian band-tail widths. These results were derived with the same capture coefficients that we used for the discrete acceptor level. For the conduction-band tail we have used here the same parameters that were used in the simulations that led to Figs. 2–8. As we see, the $G_{v0}=3\times10^{-2}$ eV case is the one that yields the best fit. However, as in the case of Fig. 3, we have, as far as the strength of the temperature dependence of the above properties is concerned, a poor quantitative agreement with the results of Fig. 1. Again, as in the discrete acceptor case, we got a significant improvement in the quantitative agreement with the experimental results by assuming that the capture coefficient of the electrons in the centers of the valence-band-tail states, C_{nv}, increases with increasing temperatures as $(T/300)^3$. Indeed, the corresponding results, shown in Fig. 10, exhibit the *best quantitative agreement* between the simulated results and the experimental results that we were able to obtain in this work. On the other hand, introducing only the temperature dependence of the mobility, or the temperature dependence of the hole capture coefficient, C_{pv}, did not yield much of an improvement.

Turning to the recombination process we show in Fig. 11, as in Fig. 7, that the charge neutrality is maintained by the compensation of the two types of neutral states of the two band tails (electrons in the conduction-band tail N_{ct} and holes in the valence-band tail P_{vt}) and that the recombination rate via the Gaussian valence-band tail, G_{vt}, dominates the recombination rate via the conduction-band tail G_{ct}. Again, we note that the results do not depend critically on the other parameters of the system. The important point is, however, that within a reasonable volume of the parameter space the experimental results can be reproduced. The corresponding scenario as exhibited by the DOS of its occupied states is illustrated in Fig. 12. As shown in Fig. 13 we can conclude that in the present scenario, as with the discrete-level acceptor scenario (Fig. 6), the experimental data suggest that there are less than 10^{15} cm^{-3} dangling bonds in our samples.

Summarizing the results presented in this section, we can conclude that the possibility to account for the experimental data of both the $\mu\tau$'s and γ's, quantitatively seems to be best fulfilled by applying a Gaussian valence-band tail. As will be discussed below this is in excellent agreement with many of
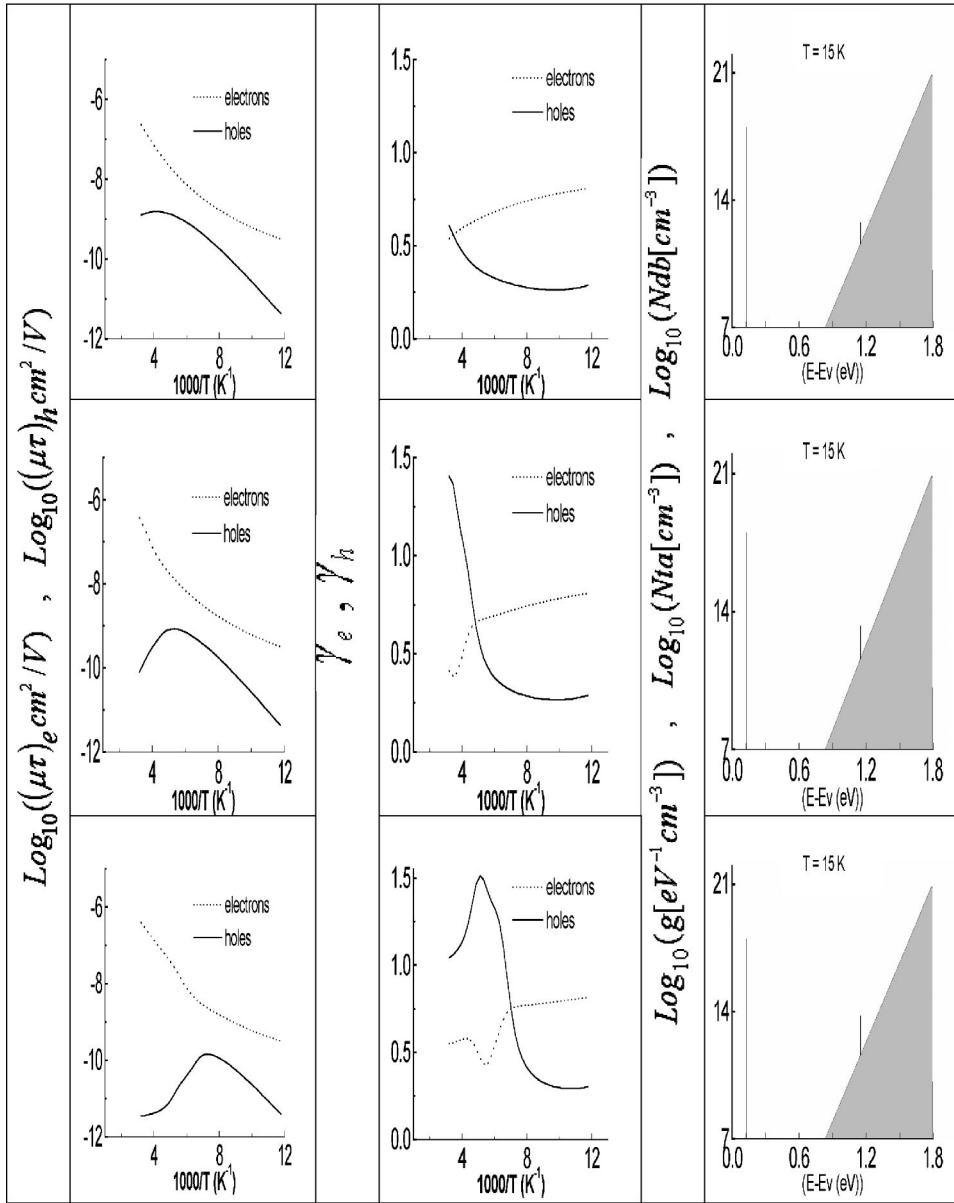
FIG. 6. The effect of the dangling bond concentration N_{db} (10^{14}, 10^{15}, 10^{16} cm^{-3}) on the behavior of the phototransport properties for a model that includes centers with a discrete level at $E_{ta} = 0.125$ eV, and a concentration of 10^{18} cm^{-3} acceptors. (Note that the concentration of the negatively charged dangling bonds is given in the right column.)

the DOS maps that were suggested for polycrystalline silicon materials.[50–57] The results of our model simulations also suggest quite convincingly that the DOS of our single-phase μc-Si:H is very different from that of a-Si:H.

VI. DISCUSSION

In this section we discuss the main advantages of our method for the derivation of DOS maps, the possible two scenarios that emerge from the findings described in Sec. V and the corresponding consequences regarding the transport and phototransport in our single-phase μc-Si:H.

A. The advantages of the present method

As we have shown in previous works[22,30] and in Sec. V, our requirement of a simultaneous agreement of the temperature dependencies of *all* four computed phototransport properties with the experimental data is quite a stringent one as

(unlike most methods) it enforces four cross self-consistency tests. This advantage of the method was manifested in the present work by our ability to conclude in Sec. V that, of the variety of possible model scenarios, there are only two that can approximate the actual DOS map in the material under study. In both scenarios there is an exponential conduction-band tail, of donorlike states, with a width of 0.03 eV. We have proven that these characteristics are robust features of the material. While no quantitative determinations of the band-tail width in μc-Si:H were reported, our results are consistent with previous works[38,58,59] that indicated the presence of localized (and in particular donorlike[59]) states adjacent to the conduction-band edge. Our findings demonstrate that our above stringent requirement enables us not only to limit the number of possible scenarios (e.g., the basic features of the DOS map) but also to narrow down the parameter space of a scenario that is found (e.g., the band-tail widths). In particular our method is proven to meet the call[26]
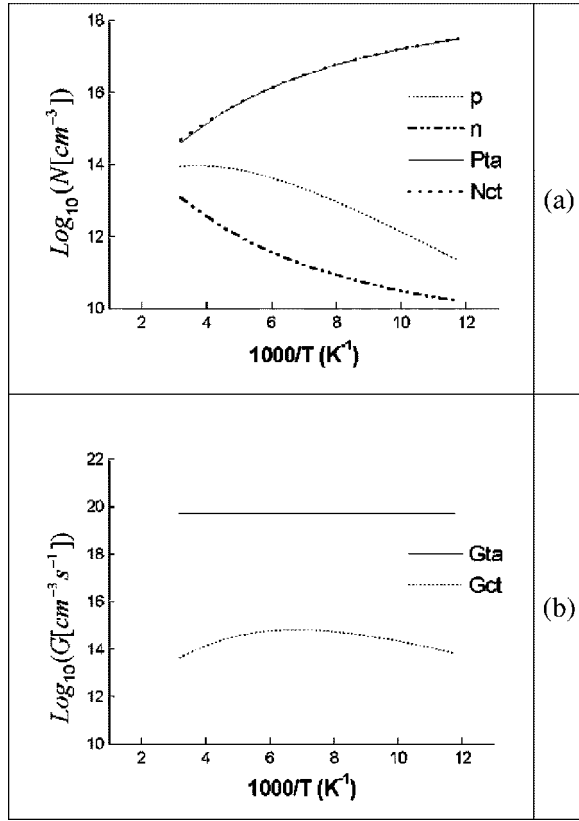
FIG. 7. The temperature dependence of the free carrier concentration (n and p) and the electron occupied states in the conduction-band tail, N_{ct}, and the concentration of the hole occupied states in the acceptors' level, P_{ta}, (a), as well as the corresponding recombination rates (G_{ct} and G_{ta}) via these states (b). This is for acceptor centers with a concentration of $N_{ta} = 10^{18}$ cm^{-3}, and a single-level energy of $E_{ta} - E_v = 0.125$ eV.
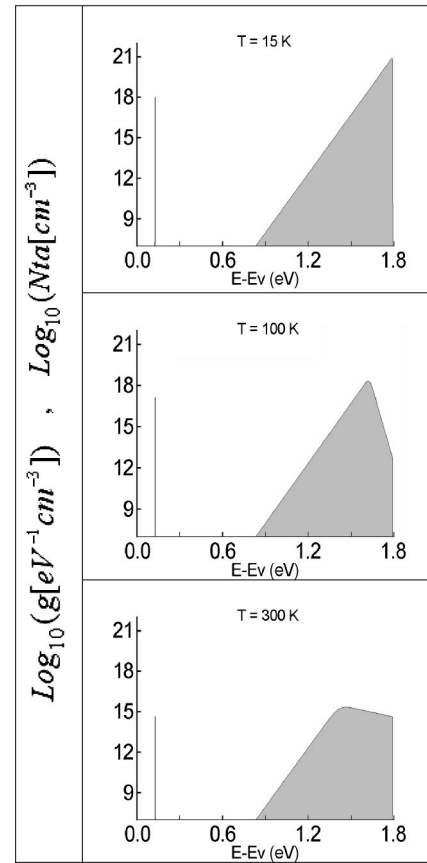

FIG. 8. The DOS map of the states that participate in a recombination process for three temperatures. This is for a system with a conduction-band tail with a width of 0.03 eV and a total acceptor concentration of $N_{ta} = 10^{18}$ cm^{-3}, with an acceptor center level at $E_{ta} = 0.125$ eV.

(and to overcome the difficulty[60]) for an experimental method that can determine (or distinguish) the shapes of the band tails. This is a clear advantage over the difficulty and complexity with other methods that were attempted[51–56,61] for the same purpose. We note, however, in passing that to obtain high certainty of the uniqueness of the fitted model, one must examine systematically and critically the effect of each parameter of the model on the results. In this sense the present approach yields a general recipe for the derivation of the DOS map but it requires the specific knowledge or at least an initial guess of the parameters.

B. The two possible scenarios

Our present work is experimental proof of how robust and well founded the Rose theory[25] is for an exponential band tail, in our case a conduction-band tail. On the other hand, for the state distribution in the vicinity of the valence band we found two scenarios. One is that of single-level acceptor-like centers that lie 0.125 eV above the valence-band edge, and the other of a Gaussian valence-band tail that has a width of 0.03 eV. Another finding in our study is that our experimental results indicate the absence of dangling bonds. In particular, our simulations show that, for both scenarios, if

there are dangling bonds in our samples, their concentration is lower than 10^{15} cm^{-3}. Following these results, but considering the many works[29,62,63] on heterogeneous μc-Si:H, we must conclude that the dangling bonds discovered in those works are due to the a-Si:H phase embedded in the corresponding samples. For example, the suggestion[64] that at high temperatures the recombination involves dangling bonds, while at low temperature it involves only band-tail states, was derived for a material that consists of 25 vol. % of a-Si:H. Since this is also the scenario[36] in a-Si:H, it is not unexpected that the latter phase dominates the recombination in heterogeneous μc-Si:H. We can thus safely assume that the single-phase μc-Si:H has, except for the width of its conduction-band tail, a very different DOS map than a-Si:H.

The issue that arises from the fact that we have, in principle, two plausible scenarios for the DOS map is which of them is the more likely one. We saw that the data can be well fitted in the vicinity of E_v by either the single-level centers or the Gaussian band-tail centers. While the existence of the former cannot be ruled out completely, there are quite a few arguments that support the second scenario. First, for reasonable values of N_{ta}, the overall agreement between the model simulations and the experimental data was better with the Gaussian band tail than with the single-level centers. Also,
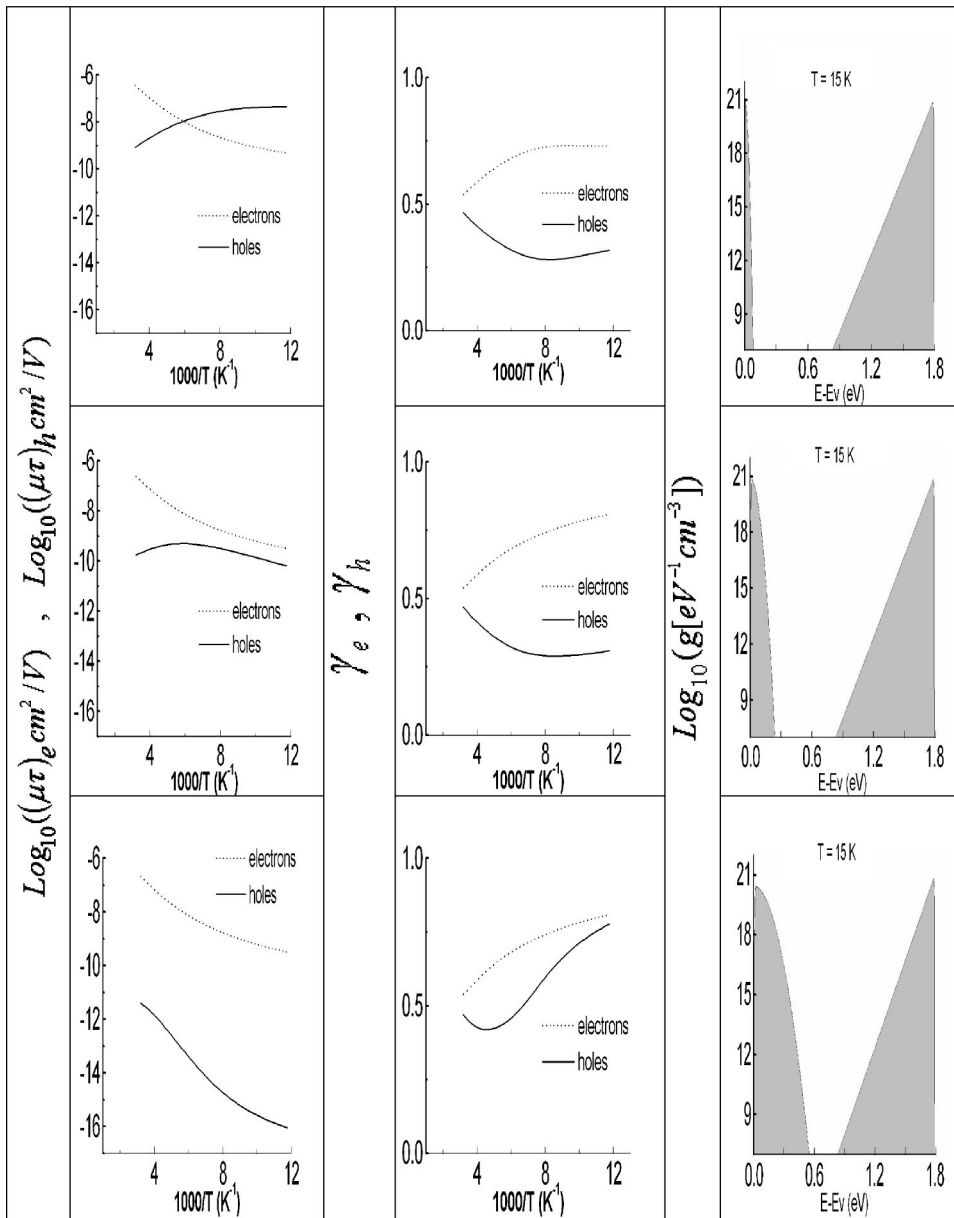
FIG. 9. The simulated temperature dependence of the four phototransport properties for three widths (0.01, 0.03, and 0.07 eV) of the Gaussian valence-band tail.

the reasonable good agreement with the single-level-like centers can be interpreted as due to the fact that this single level is simply an effective representation of the Gaussian band tail that actually exists. Third, we know that in polycrytalline silicon,[50–57] which is a "more ordered" system than μc-Si:H, there is a valence-band tail, rather than a single-level center, that accounts for very many data. In fact, two band tails are usually concluded in those systems. In some polycrystalline silicon materials a Gaussian-like conduction-band tail has been reported,[56] and in others a Gaussian-like valence-band tail has been suggested.[55] Concluding from the above discussion that a Gaussian-like band tail is the more likely scenario, we note in passing that while initially Gaussian band tails were suggested only theoretically,[48] in recent years such band tails have been proven experimentally for organic[65] and inorganic semiconductors.[46] The finding of a Gaussian band tail is of quite general importance since the transport and phototrans-

port mechanisms in such a band tail may be quite different than in exponential band tails.[46,48,66] This Gaussian band tail may be the reason for the very low mobility values that we found for the holes compared to what we found in the exponential band tail for the electrons (see Sec. V). It is of no surprise that *the electrons and the holes conduct via different mechanisms in our single-phase μc-Si:H (see below). The* latter conclusion is also in accordance with the findings in polycrystalline silicon for which low-temperature transport in the band tails and higher-temperature conduction in the bands themselves have been suggested.[57] We see then that our conclusion concerning the state distribution in single-phase μc-Si-H is more reminiscent of that of polycrystalline silicon than that of a-Si:H. This conclusion does not apply, however, when we consider the character of the band-tail states. For polycrystalline silicon it was usually concluded[53] that the conduction-band-tail states have an acceptorlike character while the valence-band-tail states have a donorlike
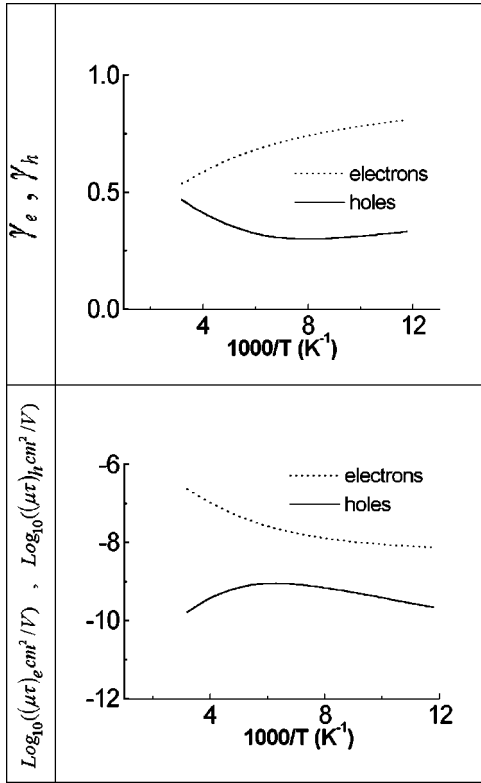
FIG. 10. The simulated temperature dependence of the four phototransport properties in an attempt to get a quantitative fit to the experimental data shown in Fig. 1. This is for the case of a Gaussian valence-band tail, with a width of 3×10^{-2} eV and a temperature-dependent capture coefficient of the electrons in this band tail.

FIG. 11. (a) The temperature dependence of the free carriers concentrations (n and p), the electron occupied states in the conduction-band tail, N_{ct}, and the concentration of hole occupied states, in the Gaussian valence-band tail, P_{vt}. (b) The temperature dependence of the recombination rates via the band-tail states (G_{ct} and G_{vt}) for a Gaussian valence band tail with a width of $G_{v0} = 3 \times 10^{-2}$ eV. This is under the conditions used in the derivation of Fig. 10.

character. This is not the case for a-Si:H where the character of the band-tail states is not well established at this date and different characters of these states have been proposed in different studies.[35,36]

The above conclusions suggest that the crystallite-encapsulating layer in μc-Si:H is different from that of the grain boundaries in polycrystalline silicon and that of homogeneous a-Si:H. This conclusion may be explained by the recent finding that the features of the Si—H bonds and the effect they impose on their neighborhood may be common to various hydrogenated silicon systems[67–69] and that they may be due to the bond bending[70] that is associated with the "surface character" of the defects in the encapsulating layer. This is in contrast to the "bulk character" of the bonds in homogeneous a-Si:H. In particular, it appears that while the state distribution is determined by the structural disorder in the disordered layer, it is the hydrogenation[6,71] that may turn around the character of the states.

C. The transport and phototransport in single-phase μc-Si:H

Let us consider now the consequences of our spectroscopic findings on the understanding of the transport and phototransport mechanisms in single-phase μc-Si:H. The effect of the state distribution on these processes in disordered semiconductors has been considered by quite a few authors[46,48,66,71,72] and some of them[13,64] emphasized the role
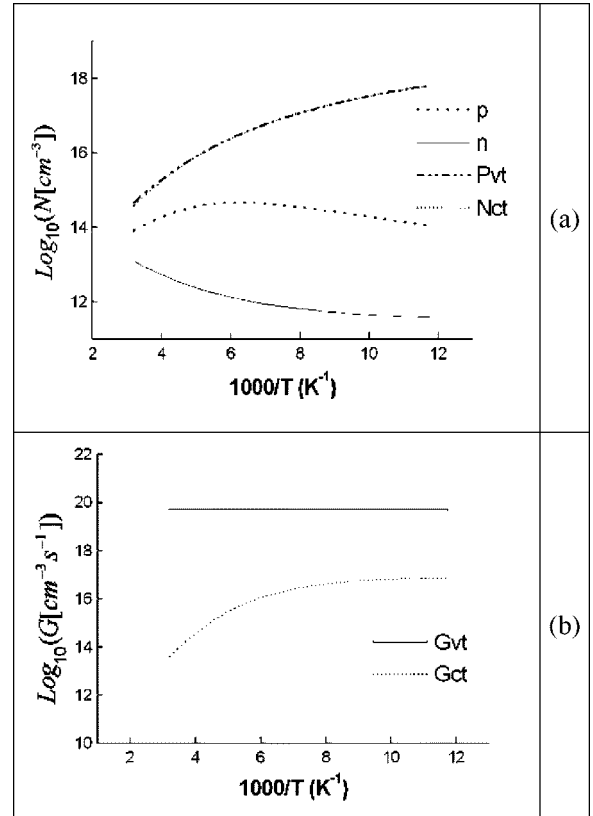
of the band tails on the conduction process in μc-Si:H. We have concluded in the above discussion that the exponential band tail with donorlike states and the Gaussian valence-band tail with "unspecified" character states originate from the disordered silicon layer. Considering the fact that both our structural and phototransport analyses do not reveal an a-Si:H phase we can conclude that our samples consist of silicon crystallites and their boundaries, and thus we may ignore models of μc-Si:H/a-Si:H mixtures. In the most common model to explain the transport in these systems[2,8] the transport takes place within the crystallites and then by tunneling[20] or thermal emission[73] between the crystallites. Our results are consistent with the alternative interpretation,[8] i.e., that the phototransport is carried out throughout the continuous network of the boundaries. This is because the phototransport is dominated by a disordered silicon layer and because the hole mobility that we concluded is very small compared to that of polycrystalline silicon and even a-Si:H. In fact, the large μ_e/μ_h ratio was already suggested[74] to be the signature of a disordered system, while a small ratio was suggested to be the fingerprint of intercrystallite transport. The inherent asymmetry that we found in the band tails provides an explanation for the asymmetry in the mobility val-
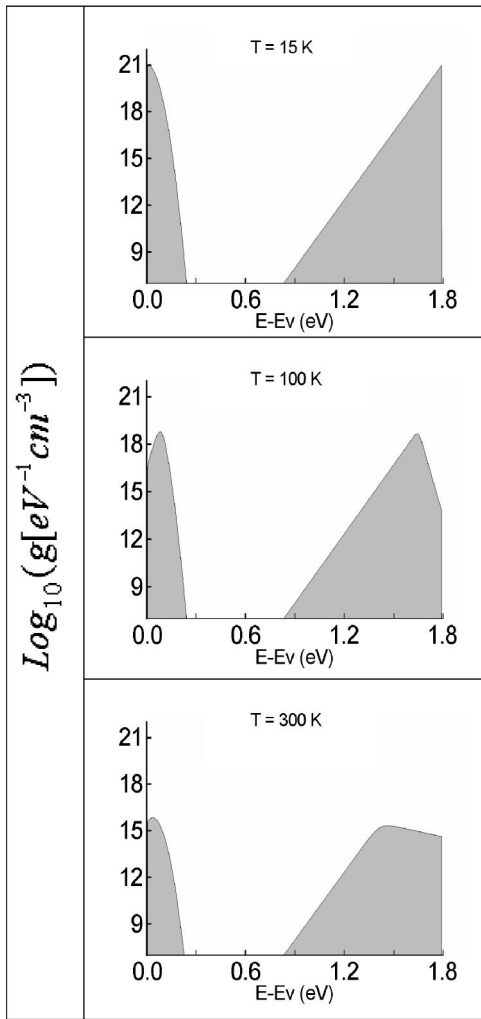
FIG. 12. The DOS map of the centers that participate in the recombination for three temperatures. This is for the case of a Gaussian valence-band tail that yielded the behaviors presented in Fig. 10.

ues of the two charge carriers. For the electrons the corresponding conduction-band tail (which is very reminiscent of that in a-Si:H) enables extended state conduction[24,71] with mobility values similar to those found in a-Si:H.[32,71] In contrast, for the holes, the low mobility can be associated with the conduction between localized states in general[71] and hopping conduction (that is manifested by very small mobility values[71,72]) at the transport energy level[75] in particular. The latter may coincide with the "single effective" level of the centers that we found to represent the Gaussian valence-band tail.

The fact that our phototransport data results are consistent with the transport and recombination in the disordered "grain boundary" silicon layer raises the question of the location of the carrier photogeneration. It turns out that optical absorption measurements on microcrystalline silicon, with crystallite sizes such as in our samples, suggest that about 40% of the light absorption takes place in the disordered silicon layer.[19] In the corresponding study this layer was estimated to be 18 Å thick, and to have an intermediate absorp-

tion between that of crystalline silicon and that of a-Si:H. These findings further suggest that the carrier generation that we use in our phototransport measurements takes place in the layer rather than in the crystallites.

Motivated by the above conjecture regarding the transport route we have turned to its direct test by applying local scanning techniques. We have applied scanning tunneling microscopy (STM) and conductance atomic force microscopy (C-AFM) in order to find whether the main current route is via the disordered layer or via the crystallites. The results that we obtained[76] by both techniques and on both sets of samples do indeed confirm the possibility that we conjectured from the DOS that we derived, i.e., that the transport takes place in the disordered silicon layer.

As for the heterogeneous μc-Si:H system, it is expected[77] that as the crystallites become larger, there will be a transition from the layer transport, suggested here, to the one encountered in polycrystalline silicon. Since these two types of transport are different from those of a-Si:H our results also resolve then the "striking similarities of μc-Si:H and a-Si:H" that were claimed[58] previously. It appears that such conclusions that were derived on heterogeneous systems were associated mainly with the a-Si:H phase that exists there.

In conclusion, in addition to the main result of this work, i.e., the derivation of the DOS map in single-phase μc-Si:H, we were able to suggest that the transport and phototransport take place in the disordered silicon layer that wraps the crystallites. The conduction mechanism is that of transport in extended states for the electrons and that of hopping conduction between localized states for the holes. We also found that our specific findings have some general consequences for the basic physics of disordered semiconductors in general and for chalcogenide glasses, organic semiconductors, polycrystalline systems, and porous silicon networks in particular. In all these cases, band tails in general and Gaussian band tails in particular seem to be present, showing that extended states and hopping conduction may dominate not only the transport but also the phototransport in them.

APPENDIX: THE VALUES OF THE PARAMETERS USED IN THE SIMULATIONS

The parameters used in our models, in Sec. V, unless specified otherwise, were as follows. Starting with the band gap of the system, E_g, we realize that it has not been studied previously for single-phase μc-Si:H. On the other hand, values between that of c-Si (i.e., 1.1 eV) and that of a-Si:H (i.e., 1.8 eV) have been reported[13,19,62,64,78] for multiphase μc-Si:H, and thus we could not pinpoint its value for our single-phase samples. Since we did not find any significant effect of the particular choice within the above range of plausible E_g values and since our preliminary conclusion was
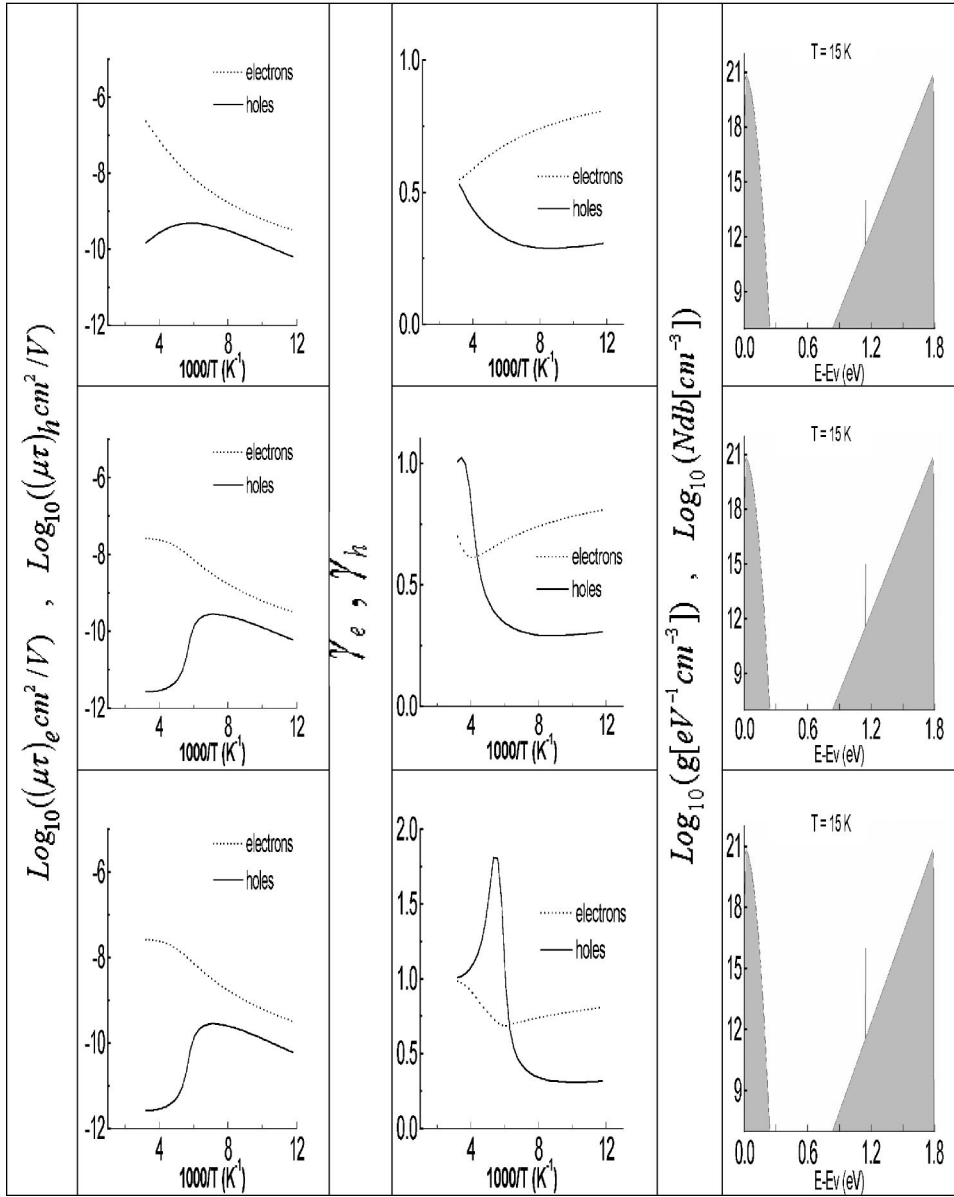
FIG. 13. The effect of the dangling-bond concentration on the behavior of the phototransport properties for the case of a Gaussian valence-band tail with a width of $G_{v0} = 3 \times 10^{-2}$ eV and acceptorlike centers. This is for the conditions that yielded the results shown in Fig. 9 for the same G_{v0} and for the dangling bond concentrations $N_{db} = 10^{14}$, 10^{15}, and 10^{16} cm^{-3}.

that the phototransport of the electrons takes place in a disordered hydrogenated silicon tissue, we adopted the 1.8 eV value of a-Si:H for E_g and $E_v + 1.3$ eV for E_F (see Sec. III) as the common parameters in our simulations. Similarly, for the multiphase μc-Si:H reported[7,74,79] values for the effective (Hall and drift) electron mobility, μ_e, range from the order of 0.1 to the order of 50 cm^2/V sec. However, generally, temperature-independent values[13] of the order of 1 cm^2/V sec were concluded[5,16,41,73] for "intrinsic" μc-Si:H. We have assumed (unless specified otherwise) a temperature-independent constant value of 1 cm^2/V sec for the electrons in our system. For the value of the hole mobility, μ_h, the estimates range from about 10 times[5,79] to 200 times[41] smaller than that of the electrons. However, the proximity of the former ratio to the ratio common for a-Si:H (Refs. 36 and 80) suggests that this value may have to do with the latter phase. Our approach was to take the value of μ_h as the value that fits best our experimental phototransport data.

In our model the effective density of states at the band

edges (E_c and E_v) N_c and N_v were taken for simplicity to be a constant with the known value of crystalline silicon[44] and other silicon systems,[36] i.e., 2.5×10^{19} cm^{-3}. In view of the discussion in Secs. III, IV, and V, the corresponding conduction-band tail was assumed to have an exponential state distribution with a density of states of $N_{ct0} = 10^{21}$ cm^{-3} eV^{-1} (at E_c) and a width, E_{c0}, of 0.03 eV. For the valence-band tail we assumed $N_{vt0} = 10^{21}$ cm^{-3} eV^{-1} and considered mainly the Gaussian distribution with the best-fit width, G_{v0}, of 0.03 eV. The capture coefficient for the electrons for the corresponding donor states in the conduction-band tail, C_{nc} [see C_n in Eq. (7)], was taken to be much larger than that for the holes, C_{pc} (see below). This assumption of evident donorlike states was borne out, as described in Sec. V, from our findings. For the other states that were included in our simulation model the standard parameters of the centers of the discrete acceptor level were derived as follows. First, the energetic position of this level, $E_{ta} - E_v$, was chosen by the best fit as 0.125 eV. Second,

with no available *a priori* values for the capture coefficients in the single-phase μc-Si:H the preliminary orders of magnitude of the capture coefficients were taken as those estimated for crystalline, amorphous,[36] or polymorphous silicon.[81] Following many trials for the best fit with the experimental data we have chosen the following parameters as our standard set. The capture coefficient for the electrons in the conduction-band tail, C_{nc}, was taken to be 10^{-9} cm^3 sec^{-1} while the capture coefficient for the holes in this tail, C_{pc}, was taken to be 10^{-15} cm^3 sec^{-1}. When valence-band-tail states with various distributions were considered, we found the results to be insensitive to the character of the states. However, for the presentation given here, we show only the results that were obtained when we assumed acceptorlike states. The corresponding discrete or band-tail capture coefficients that we have assumed were, respectively,

C_{na} or $C_{nv}=10^{-8}$ cm^3 sec^{-1} for the electrons, and C_{pa} or $C_{pv}=10^{-6}$ cm^3 eV^{-1} for the holes.

The other possible types of band tails that we have tested were "exponential square-root tails" (which we defined by $N_{vt}(E)=N_{vt0}\exp\{-[(E-E_v)/S_{v0}]^{1/2}\}$), and steplike tails (which is defined by $N_{vt}(E)=N_{vt0}$, for the range $E_v \leq E \leq E_v+W_v$ and $N_{vt}(E)=0$ otherwise, where W_v is the "width" of this tail. When dangling bonds were added to the models, we have used for them the parameters of the standard (B1) model of Tran,[36] i.e., that the energetic position of the dangling bond is $E_{db}-E_v=0.75$ eV, that the correlation energy U is 0.4 eV, that the capture coefficients of the neutral dangling bond are $C_{n0}=C_{p0}=3\times10^{-9}$ cm^3 sec^{-1}, and that the capture coefficients of the charged dangling bonds are $C_{n+}=C_{p-}=3\times10^{-8}$ cm^3 sec^{-1}.

[1] For a general review see R. E. I. Schropp and M. Zeman, *Amorphous and Microcrystalline Silicon Solar Cells: Modeling, Materials and Device Technology* (Kluwer, Boston, 1998).

[2] For a recent review on the transport in μc-Si:H, see J. Kocka, H. Stuchlikova, J. Stuchlik, B. Rezek, V. Svrcek, P. Fojtik, I. Pelant, and A. Fejfar, in *Polycrystalline Semiconductors VI*, Vols. 80–81 of Solid State Phenomena, edited by O. Bonnard, T. Mohammed-Brahim, H. P. Strack, and J. H. Werner (Scitech, Uettikom, 2001), p. 213.

[3] For many recent papers on the properties of μc-Si:H and chalcogenides, see J. Non-Cryst. Solids 266-269 (2000); **299-302** (2002).

[4] See for example, F. Finger, C. Malten, P. Hapke, R. Carius, R. Fluckiger, and H. Wagner, Philos. Mag. Lett. **70**, 247 (1994).

[5] R. Bruggemann and C. Main, Phys. Rev. B **57**, 15080(R) (1998).

[6] Y. Lubianiker, J. D. Cohen, H.-C. Jin, and J. R. Abelson, Phys. Rev. B **60**, 4434 (1999).

[7] G. Juska, K. Arlauskas, M. Viliunas, and J. Kocka, Phys. Rev. Lett. **84**, 4946 (2000).

[8] D. Will, C. Lerner, W. Fuhs, and K. Lips, in *Amorphous and Microcrystalline Silicon Technology–1997*, edited by S. Wagner, M. Hack, E. A. Schiff, R. Schropp, and I. Shimuzu MRS Symposia Proceedings No. 467 (Materials Research Society, Pittsburgh, 1997), p. 239

[9] For a comprehensive review on the structural properties of μc-Si:H, see L. Houben, M. Luysberg, P. Hapke, R. Carius, F. Finger, and H. Wagner, Philos. Mag. A **77**, 1447 (1998); M. Tzolov, F. Finger, R. Carius, and P. Hapke, J. Appl. Phys. **81**, 7376 (1997).

[10] B. G. Budaguan, A. A. Aivazov, A. G. Radoselsky, and A. A. Popov (Ref. 8), p. 239.

[11] C. Droz, M. Goerlitzer, N. Wyrsch, and A. Shah, J. Non-Cryst. Solids **266-269**, 319 (2000), and references therein.

[12] A. G. Kazanskii, H. Mell, E. I. Terukov, and P. A. Fonsh, Semiconductors **34**, 367 (2000).

[13] R. Carius, F. Finger, U. Backhausen, M. Luysberg, P. Hapke, L. Houben, M. Otte, and H. Overhof, in *Amorphous and Microcrystaline Silicon Technology–1997*, edited by S. Wagner, M. Hack, E. A. Schiff, R. Schropp, and I. Shimuzu, MRS Symposia Proceedings No. 467 (Materials Research Society, Pittsburgh, 1997), p. 283; H. Overhof, M. Otte, M. Schmidtke, U. Backhausen, and R. Carius, J. Non-Cryst. Solids **227−230**, 992 (1998).

[14] R. Bruggemann, J. P. Kleider, C. Longeaud, D. Mencaraglia, J. Guillet, J. E. Bour'ee, and C. Niikura, J. Non-Cryst. Solids **266-269**, 258 (2000); T. Unold, R. Buggermann, J. P. Kleider, and C. Longeaud, *ibid.*, **266-269**, 325 (2000); J. P. Kleider, C. Longeaud, R. Buggermann, and F. Houze, Thin Solid Films **383**, 57 (2001).

[15] T. Kamiya, K. Nakahata, Y. T. Tan, Z. A. K. Durrani, and I. Shimizu, J. Appl. Phys. **89**, 6265 (2001).

[16] K. Shimakawa, J. Non-Cryst. Solids **266-269**, 223 (2000).

[17] G. Lucovsky and H. Overhof, J. Non-Cryst. Solids **164-166**, 973 (1993).

[18] Y. Lubianiker, J. D. Cohen, G. Lubensky, Y. Rosenwaks, J. Yang, and S. Guha, J. Non-Cryst. Solids **266−269**, 253 (2000).

[19] See, for example, F. Diehl, M. Scheib, B. Schroder, and H. Oechsner, J. Non-Cryst. Solids **227-230**, 973 (1998).

[20] See, for example, P. Hapke, F. Finger, R. Carius, H. Wagner, K. Prasad, and R. Fluckiger, J. Non-Cryst. Solids **164-166**, 981 (1993); P. Hapke, U. Backhausen, R. Carius, F. Finger, and S. Ray, in *Amorphous Silicon Technology–1996*, edited by M. Hack, E. A. Schiff, S. Wagner, R. Schropp, and A. Matsuda, MRS Symposia Proceedings No. 420 (Materials Research Society, Pittsburgh, 1996), p. 789.

[21] R. B. Wehrspohn, M. J. Powell, S. C. Deane, I. D. French, and P. Roca i Cabarrocas, Appl. Phys. Lett. **77**, 750 (2000).

[22] I. Balberg, R. Naidis, L. F. Fonseca, S. Z. Weisz, J. P. Conde, P. Alpuim, and V. Chu, Phys. Rev. B **63**, 113201 (2001).

[23] For pioneering work see M. H. Cohen, H. Fritzsche, and S. R. Ovshinsky, Phys. Rev. Lett. **22**, 1065 (1969).

[24] For a recent collection of reviews see Vol. 3 of J. Optoelectron. Adv. Mater. in particular see I. Balberg, *ibid.* **3**, 587 (2001).

[25] A. Rose, *Concepts in Photoconductivity and Allied Problems* (Interscience, New York, 1963).

[26] S. K. O'Leary and P. K. Lim, Solid State Commun. **101**, 513 (1997).

[27] Y. Lubianiker and I. Balberg, Phys. Rev. Lett. **78**, 2433 (1997); M. Rashotko and I. Balberg, Appl. Phys. Lett. **78**, 763 (2001).

[28] P. Brogueira, V. Chu, and J. P. Conde, in *Amorphous Silicon Technology–1996*, edited by M. Hack, E. A. Schiff, A. Madan, M. Powell, and A. Matsuda, MRS Symposia Proceedings No. 377 (Materials Research Society, Pittsburgh, 1995), p. 57; P. Alpuim, V. Chu, and J. P. Conde, J. Appl. Phys. **86**, 3812 (1999), and references therein.

[29] F. Finger, J. Muller, C. Malten, R. Carius, and H. Wagner, J. Non-Cryst. Solids **266-269**, 511 (2000).

[30] Y. Lubianiker, I. Balberg, and L. F. Fonseca, Phys. Rev. B **55**, R15997 (1997).

[31] I. Balberg and R. Naidis, Phys. Rev. B **57**, R6783 (1998); I. Balberg, R. Naidis, M.-K. Lee, J. Shinar, and L. F. Fonseca, Appl. Phys. Lett. **79**, 197 (2001).

[32] H. Overhof and P. Thomas, *Electronic Transport in Hydrogenated Amorphous Semiconductors* (Springer-Verlag, Berlin, 1989).

[33] R. H. Bube, *Photoelectronic Properties of Semiconductors* (Cambridge University Press, Cambridge, 1992).

[34] I. Balberg, J. Appl. Phys. **75**, 914 (1994).

[35] M. Hack, S. Guha, and M. Shur, Phys. Rev. B **30**, 6991 (1984).

[36] For a detailed discussion of experimental results and simulations of the phototransport properties in *a*-Si:H-like materials, as well as corresponding references, see M. Q. Tran, Philos. Mag. B **72**, 35 (1995).

[37] M. Heintze, R. Zellitz, H. N. Wanka, and M. B. Schubert, J. Appl. Phys. **79**, 2699 (1996).

[38] R. Schwarz, T. Murias, J. P. Conde, P. Brogueira, and V. Chu, in *Amorphous and Microcrystalline Silicon Technology–1998*, edited by R. Schropp, H. M. Branz, M. Hack, I. Shimuzu, and S. Wagner MRS Symposia Proceedings No. 507 (Materials Research socity, Pittsburgh, 1998), p. 799, and references therein.

[39] R. Vanderhaghen, S. Kasouit, R. Brenot, V. Chu, J. P. Conde, F. Liu, A. de Martino, and P. Roca i Cabarrocas, J. Non-Cryst. Solids **299-302**, 365 (2002).

[40] Y. Chen and S. Wagner, Appl. Phys. Lett. **75**, 1125 (1999).

[41] I.-C. Cheng and S. Wagner, Appl. Phys. Lett. **80**, 440 (2002).

[42] For a recent discussion see O. Bleibaum, H. Bottger, and V. V. Bryksin, Phys. Rev. B **56**, 6698 (1997), and references therein.

[43] W. H. Press, B. P. Flannery, S. A. Teukolsky and W. T. Vetterling, *Numerical Recipes* (Cambridge University Press, Cambridge, 1986), Chap. 9.

[44] R. Smith, *Semiconductors* (Cambridge University Press, Cambridge, 1961).

[45] For a comprehensive review see P. T. Landsberg, *Recombination in Semiconductors* (Cambridge University Press, Cambridge, 1991), Chap. 2, and references therein.

[46] V. I. Arkhipov, E. V. Emilianova, and G. J. Adriaenssens, Phys. Rev. B **64**, 125125 (2001); V. I. Arkhipov and G. J. Adriaenssens, *ibid.* **54**, 16696 (1996); D. V. Nikolaenkov, V. I. Arkhipov, and V. R. Nikitenko, Semiconductors **34**, 655 (2000); and references therein. For the temperature dependence of the states distribution in band tails, see D. A. Drabold, in *Properties and Applications of Amorphous Materials*, edited by M. F. Thorpe and L. Ticky (Kluwer, Dordrecht, 2001); V. I. Arkhipov, G. J. Adriaenssens, and B. J. Yan, Solid State Commun. **100**, 471 (1996); S. Grabtchak and M. Cocivera, Phys. Rev. B **60**, 10997 (1999).

[47] F. Wang and R. Schwarz, Phys. Rev. B **52**, 14586 (1995).

[48] For earlier works see, S. Abe and Y. Toyozawa, J. Phys. Soc. Jpn. **50**, 2185 (1981); E. N. Economou, C. M. Soukoulis, M. H. Cohen, and A. D. Zdetsis, Phys. Rev. B **31**, 6172 (1985).

[49] A. A. Klochikhin and S. G. Ogloblin, Phys. Rev. B **48**, 3100 (1993); A. A. Klochikhin, *ibid.* **52**, 10979 (1995).

[50] For an earlier collection of reviews, see *Polycrystalline Semiconductors*, edited by G. Harbeke (Springer-Verlag, Berlin, 1985).

[51] O. K. B. Lui, S. W. B. Tam, P. Migliorato, and T. Shimoda, J. Appl. Phys. **89**, 6453 (2001).

[52] G. A. Armstrong, J. R. Ayres, and S. D. Brotherton, Solid-State Electron. **41**, 835 (1997).

[53] J. R. Ayres, J. Appl. Phys. **74**, 1787 (1993).

[54] S. S. Chen and J. B. Kuo, J. Appl. Phys. **79**, 1961 (1996).

[55] T. J. King, M. G. Hack, and I. W. Wu, J. Appl. Phys. **75**, 908 (1994).

[56] C. A. Dimitriadis, J. Appl. Phys. **73**, 4086 (1993).

[57] S. Ishida, S. Takaoka, K. Oto, K. Murase, S. Shirai, and T. Serikawa, J. Non-Cryst. Solids **200**, 1125 (1996); Appl. Surf. Sci. **114**, 685 (1997).

[58] W. Fuhs, P. Kanschat, and K. Lips, J. Vac. Sci. Technol. **18**, 1792 (2000).

[59] S. Brehme, P. Kanschat, T. Weis, K. Lips and W. Fuhs, in *Polycrystalline Semiconductors VI*, Vols. 80–81 of Solid State Phenomena, edited by O. Bonnard, T. Mohammed-Brahim, H. P. Strack, and J. H. Werner (Scitech, Uettikom, 2001), p. 225.

[60] D. P. Webb, C. Main, S. Reynolds, Y. C. Chan, Y. U. Lam, and S. K. O'Leary, J. Appl. Phys. **83**, 4782 (1998); S. Grabtchak, C. Main, and S. Reynolds, J. Non-Cryst. Solids **266**, 362 (2000).

[61] C. Longeaud and J. P. Kleider, Phys. Rev. B **45**, 11672 (1992).

[62] S. Hamma and P. Roca i Cabarrocas, Appl. Phys. Lett. **74**, 3218 (1991).

[63] For a recent work see for example, A. L. Baia Neto, A. Lambertz, R. Carius, and F. Finger, J. Non-Cryst. Solids **299-302**, 274 (2002).

[64] P. Kanschat, K. Lips, and W. Fuhs, J. Non-Cryst. Solids **226-269**, 524 (2000).

[65] M. Pope and C. E. Swenberg, *Electronic Processes in Organic Crystals and Polymers*, 2nd ed. (Oxford University Press, Oxford, 1999).

[66] C. E. Neble, R. A. Street, N. M. Johnson, and J. Kocka, Phys. Rev. B **46**, 6789 (1992).

[67] S. B. Zhang and H. M. Branz, Phys. Rev. Lett. **84**, 967 (2000).

[68] R. Krankenhagen, M. Schmidt, S. Grebner, M. Poschenrieder, W. Henrion, I. Sieber, S. Koynov, and R. Schwarz, J. Non-Cryst. Solids **198-200**, 923 (1996).

[69] D. Karnia, R. P. Barclay, and J. M. Boud, J. Non-Cryst. Solids **137**, 375 (1991).

[70] H. Shirai and T. Arai, J. Non-Cryst. Solids **198-200**, 931 (1996).

[71] S. R. Elliot, *Physics of Amorphous Materials* (Longman, New York, 1990).

[72] C. Godet, Philos. Mag. B **81**, 205 (2001).

[73] P. G. LeComber, G. Willeke, and W. E. Spear, J. Non-Cryst. Solids **59-60**, 795 (1983).

[74] R. Brenot, R. Vanderhaghen, B. Drevillon, and P. Roca i Cabarrocas, J. Non-Cryst. Solids **266-269**, 336 (2000).

[75] V. I. Arkhipov, E. V. Emelianova, and G. J. Adriaenssens, J.

Phys.: Condens Matter **11**, 2531 (1999).

[76] I. Balberg, Y. Dover, D. Azulay, O. Millo, J. P. Conde, and V. Chu, in Proceedings of the 14th International Photovoltaic Science and Engineering Conference, Bangkok (to be published).

[77] B. Rezek, C. E. Nebel, and M. Stutzmann, J. Non-Cryst. Solids **266-269**, 315 (2000).

[78] D. Han, G. Yue, J. D. Lorentzen, J. Lin, H. Habuchi, and Q. Wang, J. Appl. Phys. **87**, 1882 (2000).

[79] See, for example, P. Bulkin, R. Brenot, B. Drevillon, and R.Vanderhagen, J. Non-Cryst. Solids **231**, 268 (1998); A. Heya,

A.-Q. He, N. Otsuka, and H. Matsumura, *ibid.* **227-230**, 1016 (1998).

[80] U. Haken, M. Hundbausen, and L. Ley, J. Non-Cryst. Solids **166**, 497 (1993); Y. Tsutsuni, H. Yamanoto, K. Hattora, H. Okomoto, and Y. Hanatiasu, *ibid.* **166**, 893 (1993); C. E. Nebel and R. A. Street, Philos. Mag. B **67**, 407 (1993).

[81] M. Meaudre, R. Meaudre, R. Butt'e, S. Vignoli, C. Longeaud, J. P. Kleider, and P. Roca i Cabrrocas, J. Appl. Phys. **86**, 946 (1999).